Tampere University

UZMAN ALI

COMPARISON OF CONVENTIONAL 50-OHM IMPEDANCE MATCHING AND ANTENNA SELF-MATCHING FOR ENERGY HARVESTER

Faculty of Computing and
Electrical Engineering
Master's Thesis
Oct 2019

ABSTRACT

Uzman Ali: Comparison of Conventional 50-ohm Impedance Matching and Antenna Self-Matching for Energy Harvester
Master of Science Thesis
Tampere University
October 2019
Master's Degree Program in Electrical Engineering
Major: Wireless Communication and RF Systems
Examiner: Academy of Research Fellow Toni Björninen and Doctoral Student Nikta Pournoori

In recent time, the demand of low power wirelessly operated application devices has shown a rapid growth. To energize these low power devices with conventional batteries is a significant problem because these storage devices have small lifetime. Conventional batteries do not provide continuous operation without deteriorating the performance of electronic devices because proper maintenance and replacement are required. Scavenging the energy from ambient sources to energize the low powered wireless operated devices is up-and-coming strategy. Different techniques can be adopted but the most suitable and trending technique, on which my thesis work is focused, is the radio frequency (RF) energy harvesting from ambient electromagnetic (EM) waves in European UHF RFID spectrum from 865.7 MHz to 867.7 MHz. RF energy harvesting technique is useful due to readily availability of radiation signals i.e. cellular networks, TV, radio, Wi-Fi and satellites, which are the sources of EM waves in environment. So, this technique can be considered as an auspicious solution for the replacement of conventional batteries to provide the continuous power to small wirelessly operated electronic devices over significant longer periods.

In this thesis work, the RF energy harvesting system is simulated and fabricated which is divided into two sections; RF rectifier circuit and patch antenna. Patch antenna captures the RF signals from environment and transfer it to the RF rectifier. RF rectifier circuit converts the RF power to DC and store the charge in supercapacitor. If the impedance of RF rectifier circuit and rectifying patch antenna is not complex conjugate of each other, then maximum power transfer (MPT) will not be achieved. Therefore, Impedance matching network is introduced between harvesting patch antenna and RF rectifier circuit for maximum power transfer. Our target frequency in this work is 866 MHz.

RF rectifier circuit is simulated on advance design system (ADS) and patch antenna is simulated in HFSS. RF rectifier circuit and patch antenna are fabricated on FR4 and RT/duroid 5880 substrate respectively. Performance of the whole RF energy harvesting system is showing that, at 28dBm input power level to the reader antenna with gain 12.5dBi, our system has bandwidth of 80 MHZ from 800 to 880 MHz. Output voltage of the system are above 3V, which are enough to wake up the RFID IC and for low power level applications. The maximum read range of this RF energy harvesting system is charging is 94cm. Charging speed of supercapacitor is higher around central frequency, while slower as the operational frequency moves away from central frequency. Bandwidth and charging speed can be increased by increasing the input power level.

Keywords: RF rectifier, RF energy harvesting, Patch antenna, Impedance matching network, UHF RFID spectrum

PREFACE

This Master's thesis, "Comparison of conventional 50-ohm Impedance Matching and Antenna Self-matching for Energy Harvester" is carried out in partial fulfillment of the requirement for the master's degree in Electrical Engineering with a major in 'Wireless Communications and RF Systems' at Tampere University, Tampere, Finland. All the research work during this thesis has been made Wireless Identification and Sensing Research Group (WISE).

First and foremost, I am thankful all almighty ALLAH for giving me the courage and determination to learn and completion of my master's degree here at Tampere University, Tampere, Finland.

I would like to thank my thesis examiner and supervisor, Academy Research Fellow Dr. Toni Björninen, for providing me the opportunity to work under his supervision, and for his smart ideas, support and guidance throughout the completion of this work. It is an honor to work with him.

I am grateful to Doctoral student, Nikta Pournoori for her support, guidance and assistance during simulation and measurements. I am also thankful to Doctoral student, Shahbaz Ahmad for his support and encouragement. I would also like to thank my friends Shoiab Tahir Qureshi and Adeel Mehr for their support and motivation.

Finally, I would like to say thanks to my parents, sisters and brother for their unconditional love and support to make it possible.

Tampere, Oct 2019

Uzman Ali

CONTENTS

LIST OF FIGURES

LIST OF TABLES

LIST OF SYMBOLS AND ABBREVIATIONS

AC	Alternative Current
ADS	Advance Design System
AR	Axial Ratio
CW	Continuous Wave
DC	Direct Current
DIY	Do It Yourself
DUT	Device Under Test
EDLC	Electromechanical Double Layer Capacitor
EM	Electromagnetic
EV	Electric Vehicle
FET	Field Effect Transistor
FR4	Flame Retardant 4
FNBW	First Null Beam Width
GHz	Giga Hertz
HB	Harmonic Balance
HEV	Hybrid Electric Vehicle
HFSS	High Frequency Structure Simulator
HPBW	Half Power Beam Width
I	Intrinsic layer
IEEE	Institute of Electrical and Electronics Engineers
IoT	Internet of Things
IT	Information Technology
KHz	Kilo Hertz
LAN	Local Area Network
LHCP	Left Hand Circular Polarization
LIB	Lithium Ion Battery
LIPB	Lithium Ion Polymer Battery
LSSP	Large Signal S-Parameter
MEMS	Micro Electromechanical System
MHz	Mega Hertz
PCE	Power Conversion Efficiency
PCB	Printed Circuit Board
RFID	Radio Frequency Identification
RHCP	Right hand Circular Polarization
PHEV	Pug-in Hybrid Electric Vehicle
PIN	Positive Intrinsic Negative
S-Parameter	Scattering Parameter
SPDT	Single Pole double Throw
SPST	Single Pole Single Throw
SWR	Standing Wave Ratio
RF	Radio Frequency
RFEHS	Radio Frequency energy Harvesting System
RL	Return Loss
UHF	Ultra High Frequency
UPS	Uninterrupted Power Supply
VNA	Vector Network Analyzer
WBN	Wireless Body Network
WET	Wireless Energy Transfer
WLAN	Wireless Local Area Network
WPT	Wireless Power Transfer
WSN	Wireless Sensor Network
3D	Three Dimensional

A	Ampere
A	Area
B	Magnetic flux density
C	Capacitance per unit length
c	Velocity of light
D	Directivity
dB	Decibel
E	Electric field
F	Electric force
F	Farad
f	Frequency
G	Conductance per unit length
G	Gain of antenna
H	Magnetic field
H	Henry
Hz	Hertz
I	Current
I(z)	Current wave in z direction
J	Current density
j	Imaginary unit
K	Kelvin
k	Radiation efficiency of antenna
L	Inductance per unit length
m	Meter
mm	Millimetre
n	Nano
P	Power
P_r	Received power
P_t	Transmitted power
R	Resistance per unit length
R_A	Resistance of antenna
R_L	Resistance of load
S	Siemen
T	Temperature
V	Volt
V_{th}	Threshold voltage
V(z)	Voltage wave in z direction
X_A	Reactance of antenna
X_L	Reactance of load
Z_A	Impedance of antenna
Z_L	Impedance of load
Z_o	Characteristic impedance
α	Attenuation constant
β	Propagation constant
γ	Complex propagation constant
δ	Loss factor
δ_e	Electric loss factor
δ_m	Magnetic loss factor
δ_s	Skin depth
e_c	Conduction efficiency
e_d	Dielectric efficiency
e_{cd}	Antenna radiation efficiency
e_o	Total efficiency
e_r	Mismatch or Reflection efficiency

ε	Permittivity of medium
ε_o	Permittivity of free space
ε_r	Relative permittivity
ε'	Real part of permittivity
ε''	Imaginary part of permittivity
$\eta_{matching}$	Matching efficiency
θ	Azimuthal angle in spherical coordinate system
λ	Wavelength
μ	Permeability of medium
μ_o	Permeability of free space
μ_r	Relative permeability
μ'	Real part of permeability
μ''	Imaginary part of permeability
ξ	Instantaneous field of electromagnetic wave
ρ	Electric charge density
σ	Conductivity
σ_e	Effective conductivity
τ	Power transfer coefficient
ϕ	Polar angle in spherical coordinate system
ω	Angular frequency
Ω	Ohm
Γ	Reflection coefficient
Γ^*	Conjugate-matched reflection coefficient
∞	Infinity

.

1. INTRODUCTION

In recent times, the number of low powers wirelessly operated application devices are showing a rapid growth and energizing these low power devices is a fundamental issue. To maintain the operation of these devices the conventional batteries do not provide a long lifetime. But scavenging the energy from ambient sources to energize those wireless operated devices is an auspicious strategy for it. Different approaches can be adopted, but the most suitable and trending technique on which my research work is focusing is, harvesting the RF energy from ambient electromagnetic (EM) wave source in ultra-high frequency (UHF) band. The Harvested energy is provided to any kind of wireless applications such as wireless sensor network (WSN), wireless body network (WBN), passive RFID tags and wireless charging devices. The technique of wireless power transfer (WPT) can be categorized into wireless energy transfer (WET) and harvesting, inductive coupling and magnetic resonance coupling. For inductive coupling and magnetic resonance coupling, calibration and alignment of coils/resonators is required at both ends, transmitter and receiver. Although these two techniques carry high energy density and conversion efficiency but only suitable for short distances, varies from few millimetres to few meters, because attenuation factor is the cube of the reciprocal of the distance. On the other hand, RF energy transfer method is a better approach to transfer energy in far-field region. Although it has lower power conversion efficiency (PCE) of RF to DC but a better way to transfer energy over long distances. Strength of transmitted signal is attenuated by the reciprocal of distance between transmitter and receiver. This method can be used to energize large number of devices in wide area.

In this thesis work, the main objective is to develop the RF energy harvester having impedance which is complex conjugate with the impedance of patch antenna. Conventional antennas have impedance i.e. 50 ohm which do not provide the maximum power transfer (MPT) to the RF rectifier circuit and for this purpose proper impedance matching is required. For MPT, we introduced the matching network in rectifier circuit. When impedance of harvesting patch antenna is complex conjugate of RF rectifier circuit, the maximum power transfer is occurred and efficiency of the whole RFEHS is increased. Capturing RF power at 866 MHz (UHF RFID band) is converted into DC power which is stored in super-capacitor and utilized for RF switching and energizing the RFID tag IC and different passive RFID tags related applications.

In this work, the RF energy harvesting system (RFEHS) is consists of RF power sources, antenna, impedance matching network, rectification unit and energy storage. RF power sources which provide energy in far-field region is being captured by patch antenna. An L matching impedance network is introduced which consists of two inductors. Rectification unit is key unit to covert the RF power to DC power. Different topologies like Villard voltage multiplier or Dickson charge pump can be applied for the rectification, but in this

research work Dickson 3-stage voltage charge pump technique is utilized. After studying different storage systems and comparing their advantages and disadvantages, super-capacitors are the most suitable candidate used in this work. Except the rectification unit, patch antenna is also a key component in this RFEHS, which provides maximum power transfer to the rectification unit. When impedance of load and impedance of antenna are complex conjugate of each other, maximum power transfer is achieved. Antenna designing is crucial and important part of this research because matching the impedance without passive components (capacitors or inductors) is one of the targets of this work.

Simulations of RF energy harvesting unit have done on advance design system (ADS) and for antenna designing, ANSYS HFSS is used. RF energy harvesting circuit is deployed on FR4 substrate and patch antenna is developed on RT5880 substrate. All the simulations, testing and measurements have done at 866MHz, the frequency range of European UHF RFID band. The performance of the whole RF energy harvesting system concludes that the output DC power is enough to utilize for low power applications like passive RFID tags.

This Master of Science Thesis work is followed is this way: **Chapter 2** is about basics of electromagnetic wave theory and fundamental concepts of antenna theory including description of some important antenna parameters. **Chapter 3** presents the working principal of RF energy harvesting system. RF power sources, impedance matching network, different kinds of rectifiers and energy storage devices are explained. **Chapter 4** explains the theory of RF switch in which the introduction of PIN diode, its working principal and different structures are discussed. **Chapter 5** covers the motivation of this thesis work and describes the modelling procedure, simulations and measurements. **Chapter 6** concludes the thesis work, summaries and provides future scope of thesis work.

2. FUNDAMENTALS OF ANTENNA

2.1 Electromagnetic Theory

It is very important to know about the electromagnetic fields and wave propagation for understanding the antenna theory. The term electromagnetism refers to the interaction of electric fields and magnetic fields [1]. When charge carriers are accelerating, they produce magnetic field and that fluctuating magnetic field produces fluctuating electric field. That electric field produces another magnetic field. The result is leapfrog effect in which both fields are propagate and this synergistic field known as electromagnetic field. In this chapter, the concepts of electromagnetic theory are discussed with the help of electric and magnetic fields, skin depth, wave equations and some imperative concepts relevant to transmission lines [2].

Maxwell's Model of Electromagnetism Phenomena

A set of four equations which summaries the classical theory electromagnetism is known as Maxwell equations. These Maxwell equations characterize the relation between electric field, magnetic field, electric current and electric charge. Generation mechanism of the electric and the magnetic field are explained by these equations, how they affected by each other and by current, and charges. These four equations are representation of the elementary laws of electromagnetism. Faraday's law of induction states that electric field is produced by the changing magnetic field. Ampere's circuital law states that magnetic field is generated by the changing electric field. Gauss's law for electric fields determines the electric flux fluctuations near by the moving electric charges. Gauss's law for magnetism states that the total magnetic flux passes through a closed surface is always zero and magnetic charge does not exist [1].

Electromagnetic Properties of Materials

When there is no magnetic or dielectric material is present, constitutive equations of electric induction (D), and magnetic induction field (B) are expressed as equation (2.1) and (2.2) respectively [3],

$$D = \varepsilon_o \cdot E, \tag{2.1}$$

$$B = \mu_o \cdot H, \tag{2.2}$$

where E is electric field, H is magnetic and,

ε_o= permittivity of free space, its value is $8.854 \cdot 10^{-12}\ \left[\frac{F}{m}\right]$

$\mu_o =$ Permeability of free space, its value is $4 \cdot \pi \cdot 10^{-7} \left[\frac{V \cdot s}{A \cdot m}\right]$

Relation between dielectric permittivity of free space and magnetic permeability of the free space can be expressed as,

$$c^2 = \frac{1}{\varepsilon o \cdot \mu o} \tag{2.3}$$

where c is the speed of light, and its value is $2.998 \cdot 10^8 \left[\frac{m}{s}\right]$.

When electromagnetic field interacts with dielectric or magnetic material, equations (2.1) and (2.2) can be expressed as below (2.4) and (2.5) respectively,

$$D = \varepsilon_o \cdot \varepsilon \cdot E, \tag{2.4}$$

$$B = \mu_o \cdot \mu \cdot H, \tag{2.5}$$

where ε_o and μ_o are vacuum permittivity and permeability, while ε and μ are permittivity and permeability of the material respectively. An effective way of demonstrating the dielectric loss is to consider the permittivity ε and permeability μ as a complex number expressed as (2.6) and (2.7) respectively,

$$\varepsilon = \varepsilon' - j \cdot \varepsilon'', \tag{2.6}$$

$$\mu = \mu' - j \cdot \mu'', \tag{2.7}$$

where j is imaginary unit, and $j^2 = -1$.

In microwave electronics, the dimensionless quantities relative permittivity (ε_r) and relative permeability (μ_r) are expressed as (2.8) and (2.9) respectively [4]

$$\varepsilon_r = \frac{\varepsilon}{\varepsilon_o} = \frac{\varepsilon' - j\varepsilon''}{\varepsilon_o} = \varepsilon_r{}' - j\varepsilon_r{}'' \tag{2.8}$$

$$\mu_r = \frac{\mu}{\mu_o} = \frac{\mu' - j\mu''}{\mu_o} = \mu_r{}' - j\mu_r{}'' \tag{2.9}$$

Permittivity is the property of a dielectric material which tells that how much opposition is generated by the material in order to develop the electric field. The ability of material to store energy is explained by the real part of permittivity (ε′), while the imaginary part (ε″) describes dissipated energy in the material. Permeability is the property of a dielectric material which measure the support of the formation of magnetic field. The energy storage is represented by the real part of permeability (μ') and the imaginary part (μ'')

explains the term energy loss. More, the loss tangent which describes the inherent dissipation of the medium can be represented as [5],

$$tan\delta_e = \frac{\sigma_e}{\omega\varepsilon'} \ , \tag{2.10}$$

where ω is angular frequency, δe is known as the electric loss angle and σe is the effective conductivity which is consisted of two parts. First segment (σ_s) of effective conductivity tells the static conductivity and second segment $(\omega\varepsilon'')$ demonstrates the conductivity due to applied alternating field. Relation is given below [5]:

$$\sigma_e = \sigma_s + \omega\varepsilon'' \tag{2.11}$$

By substituting the equation (2.11) into equation (2.10), the electric loss tangent $(tan\delta_e)$ depending upon the frequency can be defined as,

$$tan\delta_e = \frac{\sigma_e + \omega\varepsilon''}{\omega\varepsilon'} \tag{2.12}$$

Magnetic loss tangent $(tan\delta_m)$, same as electric loss tangent $(tan\delta_e)$, from above relations can be expressed as,

$$tan\delta_m = \frac{\mu''}{\mu'} \tag{2.13}$$

Skin Depth

At higher frequencies, the conduction of an equally current distribution through the cross section of the conductor starts changing its conduction to almost entirely towards closer to the outer surface of the conductor. Due to bulk resistivity of conductor at sufficiently higher frequencies, the RF current starts flowing at very thin layer of the conductor. Furthermore, the current concentrates nearest to the surface that abuts the highest relative dielectric constant. Lower bulk resistivity result in shallower skin. The skin depth, or the characteristic depth of penetration is expressed as [6],

$$\delta_s = \sqrt{\frac{2}{\omega\mu\sigma}} \ , \tag{2.14}$$

where δ_s is skin depth, μ is conductor magnetic permeability, ω the angular frequency of the wave and σ is the bulk conductivity.

In case of an infinitely thick conductor, the current density of a plane wave penetrating conductor can be expressed as [6],

$$J(z) = J_o e^{-z/\delta}\left(coz\left(z/\delta\right) - jsin\left(z/\delta\right)\right) \tag{2.15}$$

where J_o is the current density at the surface of conductor, perpendicular to the conductor surface.

Instead of infinitely thick conductor, an infinitely thin conductor, with an equivalent surface impedance Z_s equal to the characteristic impedance Z_{oM} of a plane wave that is propagating along z axis in conductor can be used for modeling [6],

$$Z_s = Z_{OM} = \sqrt{\frac{j\omega\mu}{\sigma}} = (1+j)\sqrt{\frac{\omega\mu}{2\sigma}} \tag{2.16}$$

The conductors having thickness much thicker than the skin depth shows almost accurate equivalent surface impedance.

Equivalent surface impedance of a conductor with thickness t can be calculated by,

$$Z_s = -jZ_{oM}\cot(kt) \tag{2.17}$$

where,

$$k = \sqrt{(-j\omega\mu\sigma)} = (i-j)\sqrt{(\omega\mu\sigma/2)} = (1-j)\frac{1}{\delta} \tag{2.18}$$

Article [6] concludes:

$$Z_s = (1-j)R_{RF}\sqrt{f}\,cot\left((1-j)R_{RF}\sqrt{f}\,\frac{1}{R_{DC}}\right), \tag{2.19}$$

where,

$$R_{RF} = \sqrt{\frac{\pi\mu}{\sigma}},$$

$$R_{DC} = \frac{1}{\sigma t},$$

f is the frequency (Hz).

By expanding equation (2.19) into exponential form, it can be seen that,

$Z_s = R_{DC}$ at low frequency
$Z_s = Z_{OM} = (1+j)\,R_{RF}\sqrt{f}$ at high frequency.

2.2 What is an Antenna?

An antenna is a fundamental component in wireless communication systems to send or receive the radio signal [2]. Antenna is a transducer that converts the electromagnetic waves from free space to a guided wave on a transmission line and vice versa. Antennas are passive devices which can be used either for transmitting or receiving the EM waves

to establish the wireless connection between transmitter and receiver. According to IEEE definition, antenna is defined as [7]:

“That part of a transmitting or receiving system that is designed to radiate or receive the radio waves”.

2.3 Radiation Mechanism

According to Maxwell equations, time varying current or acceleration (deacceleration) of charges produce the time-varying magnetic field which results into the formation of time-varying electric field simultaneously. To keep the flow of EM waves, EM field is applied through a transmission line. Since E and H field are not only perpendicular to each other and but also both are perpendicular to the direction in which wave propagates, so the EM waves will start propagating in all directions. When E field (the same is for H field) is in the same direction, the same value and the same phase in such a plane that is perpendicular to the direction of propagation, it is called a plane wave. In ideal case, when plane wave propagates in a loss-less medium, the propagation constant (γ) is purely imaginary and no attenuation occurs i.e. α=0. In case of lossy dielectric medium, the conductivity (σ) is zeo but permittivity (ε) of the medium is complex. Hence, attenuations will appear i.e. $\alpha \neq 0$ and amplitude keeps reducing while the wave propagates. In a special case, when EM wave propagates in a good conductor, conductive current is much higher than displacement current. i.e. $\sigma >> \omega \varepsilon$ [8].

Depending on the distance from antenna, radiation field is divided into three approximated regions; reactive near field, radiating near field (Fresnel Zone) and far field (Fraunhofer Zone) [2] [9] as shown in figure 1.

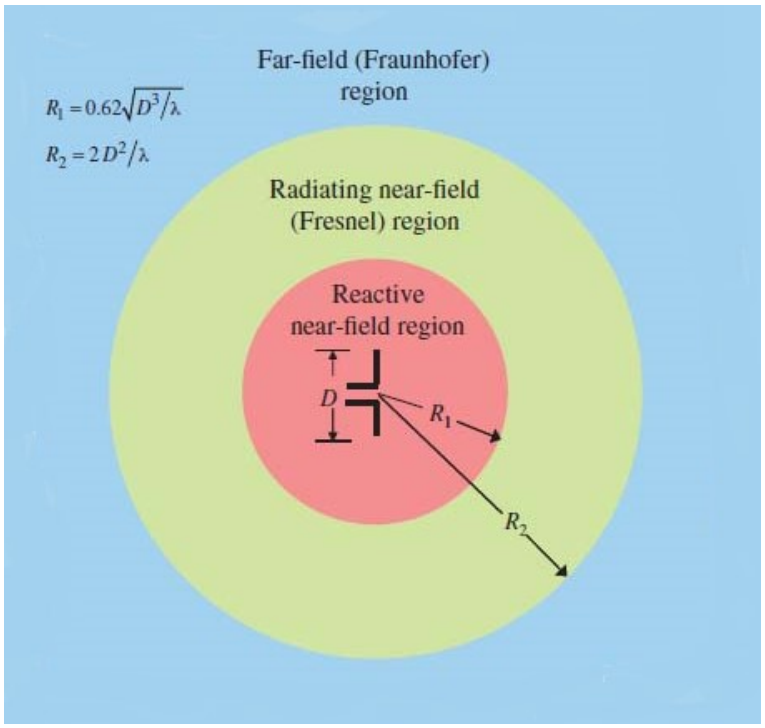

Figure 1. *Field regions of an antenna [9]*

Reactive near field region is the vicinity, where reactive filed dominates. E and H fields are not in phase and most of the energy is absorbed in this region because of no radiation. This approximated region R is,

$$R < 0.62\sqrt{\frac{D^3}{\lambda}}$$

from the antenna, where D is the largest dimension of antenna and λ is the wavelength [9] [10]. The region in between reactive near field and far field is Fresnel zone. E and H field are in phase and most of the energy radiate in this region. Its approximated region R is,

$$0.62\sqrt{\frac{D^3}{\lambda}} < R < \frac{2D^2}{\lambda}$$

In far field region, propagated waves are approximately behaving as plane waves and do not change their shape. E and H fields are in phase and perpendicular to each other and to the direction of propagation. Radiation pattern is formed in this region. It located at approximated distance R from the antenna [9] [10],

$$\frac{2D^2}{\lambda} < R < \infty$$

Furthermore, EM waves cannot propagate thorough a perfect conducting medium and bounce back [8].

2.4 Antenna Parameters

Antenna is a device, which convert the radio energy into electrical energy and vice versa. To describe the design and performance of an antenna some important parameters should be considered such as radiation pattern, input impedance, return loss and bandwidth, directivity and gain, beam width, radiation efficiency, polarization and coaxial ration. In this section, these parameters are discussed.

Directivity

Directivity is a fundamental parameter of antenna which measures the antenna power radiation in a concentrated direction as compare to its equal radiations all directions. An antenna radiates equally in all directions would have zero directionality and typically directivity would be 0dB. Directivity is the characteristic of an antenna and it is equal to gain if antenna efficiency is 100%. It is entirely determined by the pattern shape. Directivity and radiation pattern are related to each other. Directivity will be higher, if antenna radiates more in one direction. An antenna's normalized radiation pattern can be expressed as a function $F(\theta, \phi)$ in spherical coordinates.
A normalized radiation pattern is the same as a radiation pattern; it is just scaled such that the maximum value of magnitude of the radiation pattern $F(\theta, \phi)$ is equal to one.

The maximum value of directivity as a function angle $D_{(\theta,\phi)}$ can be mathematically expressed as,

$$D_{(\theta,\phi)} = \frac{1}{\frac{1}{4\pi}\int_0^{2\pi}\int_0^{\pi}|F(\theta,\phi)|^2 sin\theta d\theta d\phi} \tag{2.20}$$

This equation for directivity might look complicated, but nominator is the maximum value of F and denominator is just representing the average radiated power in all directions. Thus, the directivity can also be expressed as the ratio of maximum radiated power to the average radiated power [2].

Radiation pattern

Graphical representations of radiation received or transmitted by an antenna as a function of space coordinates. Mostly, radiation pattern determines in far field region and describes radiation properties with respect to space coordinates. Radiation pattern usually plotted in decibel (dB). For a linearly polarized antenna, performance of an antenna is depending upon the two fundamentals planes, E-plane containing E field vector and H-plane containing H field vector. Both planes are in the direction of maximum radiation. These two planes are perpendicular to each other; thus, they form a complete 3D radiation pattern in spherical coordinate system at all angles of $\theta\ and\ \phi$. However, radiation component (E_r) becomes zero in far field region. Figure 2 demonstrates the coordination system of antenna [9].

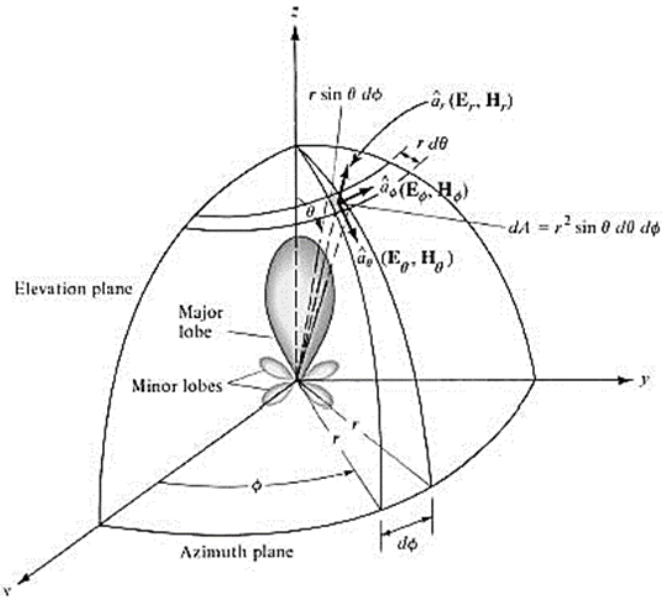

Figure 2. *Coordinate system for antenna analysis [9]*

Radiation pattern can be divided in to two parts. Major or main lobe which is in the direction of maximum radiation contains maximum power. Any other lobe than major lobe is called minor lobe, which comprise of side lobes and back lobes. Minor lobes represent the radiation pattern in any direction other than desired direction. The radiation pattern

of back lobes is in the opposite direction of the main lobe with angle 180°. Side lobes are close to main lobe with less power and can be in any direction in between the back lobe and the main lobe [9].

Beam width

The angular distance between the points of main lobe at which radiation power becomes one half of its maximum value is called half power beam width (HPBW). Similarly, first null beam width (FNBW) is the measure of an angle between first nulls of main lobe. Isotropic, directional, and omnidirectional are three categories of radiation pattern. An isotropic is an ideal pattern which radiates equally in all directions. Physically it's not realizable but valuable for comparison purposes. The directional antennas radiate effectively only in specific direction. Omnidirectional antennas are non-directional in azimuth and directional in elevation. Figure 3 demonstrates the different lobes of an antenna's radiation pattern [9].

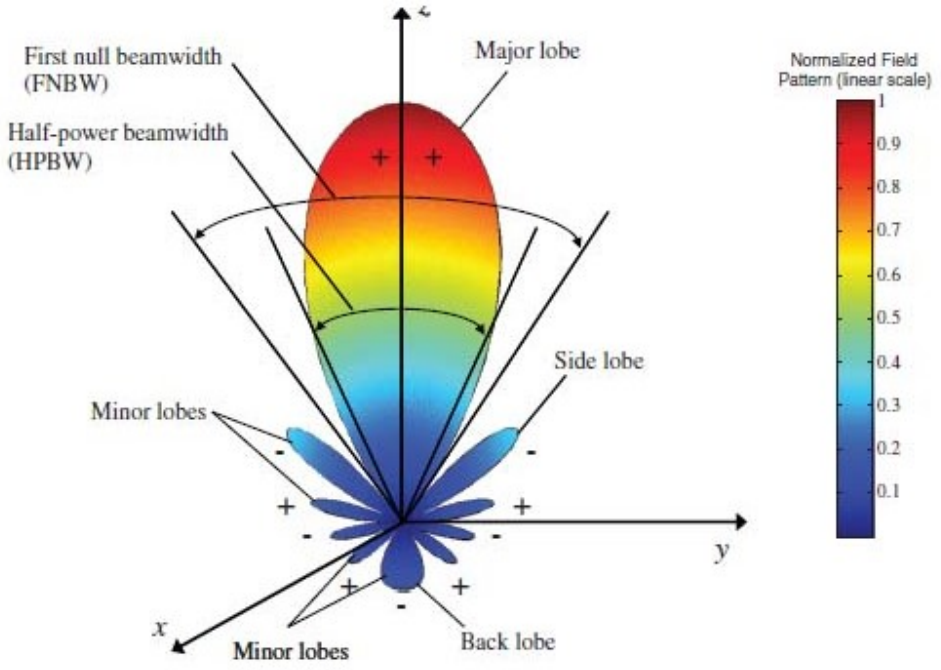

Figure 3. *Radiation pattern of an antenna with different lobes [9]*

Radiation Efficiency

Radiation efficiency is another important parameter which describes that hoe efficiently an antenna transmits and receives the RF signals. Losses may occur at the input terminals or within the antenna. Mismatching between antenna and transmission line causes reflection, ohmic losses and dielectric properties of material may affect the antenna efficiency. Generally, antenna efficiency is written as [9],

$$e_o = e_r e_c e_d \ , \tag{2.22}$$

where e_o is total efficiency, e_r is mismatching or reflection efficiency, e_c is conduction efficiency, e_d dielectric efficiency. e_c and e_d are quite hard to compute and they can be measured by experiments. Usually they are written together as e_{cd}, it is known as antenna radiation efficiency. When transmission line and antenna are matched properly, the reflection efficiency (e_r) is used to measure the power loss. e_r can be define as [9],

$$e_r = 1 - |\Gamma|^2 \tag{2.23}$$

So, the relation (2.22) can be expressed as,

$$e_o = e_r e_{cd} = e_{cd}(1 - |\Gamma|^2) \tag{2.24}$$

Gain

Gain depicts the radiation capabilities and radiation efficiency of an antenna. It can be defined as, the ration of the power gain intensity in one direction to the power gain intensity by an isotropic antenna (which radiates equally in all directions).It can be expressed as follow [2] [9],

$$G = kD, \tag{2.25}$$

where k is radiation efficiency of an antenna, and can be computed by,

$$k = \frac{P_r}{P_{in}} = \frac{P_r}{P_r + P_{loss}}, \tag{2.26}$$

where P_r is the radiation power and P_{loss} is power dissipation of an antenna.

Realized gain includes the effect of circuit losses and mismatch losses. The realized gain of an antenna is calculated by considering total efficiency of the antenna, along with its directivity. The realized gain is calculated using the total efficiency and the directivity as follows:

$$G_0\ (dB) = 10\ log_{10}(e_0 D_0) \tag{2.27}$$

Antenna Impedance and Principal of Complex Conjugate Impedance Matching

Input impedance is the ration of voltage and current at the input terminal of an antenna. Antenna input impedance is complex variable. Real part corresponds to the power either radiated or absorbed by antenna and it consist of radiation resistance (R_r) and loss resistance (R_L). The reactance part or the Imaginary part represents the energy store in near radiation field of antenna. Their relation of input impedance is expressed in (2.28). The impedance of the connected load is defined in (2.29) [9],

$$Z_A = R_A + jX_A = (R_r + R_L) + jX_A \tag{2.28}$$

$$Z_L = R_L + jX_L = (R_r + R_L) + jX_L \tag{2.29}$$

$$X_A = -X_L \tag{2.30}$$

In the transmitting mode, power generated by source will be transfer at maximum when the antenna input impedance and source impedance are complex conjugate of each other. In this condition, half of the power will be dissipated as an internal resistance in the form of heat in the antenna and other half will be delivered to antenna, of which some power dissipated by antenna. And delivered power to antenna will be totally radiate if antenna has 100 percent efficiency.

Figure 4 depicts the Thevenin equivalent circuit of on an antenna with a source in transmitter mode [9].

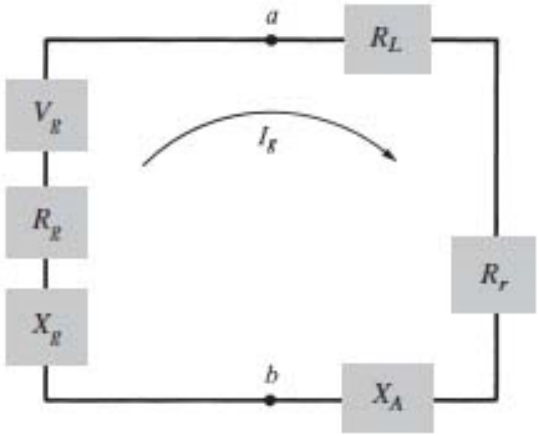

Figure 4. *Thevenin equivalent circuit of an antenna with a source in transmitting mode [9]*

In receiving mode, when antenna impedance and load impedance are complex conjugate of each other, half of the total power received by antenna is delivered to load and half of that power is scattered and dissipate as a heat resistance in antenna. Input impedance of antenna is dependents upon the frequency; therefore, impedance matching can only be achieved in a specific bandwidth. Antenna input impedance also depends upon geometry of antenna, excitation method, and materials in surroundings of antenna. Because of the complex geometry of antennas, input impedance of limited antennas is calculated analytically and mostly measured experimentally. Figure 5 shows the Thevenin equivalent circuit of an antenna with a source in receiving mode [9].

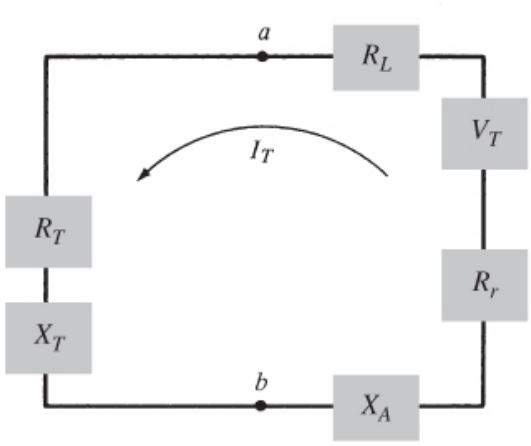

Figure 5. *Thevenin equivalent circuit of an antenna with a source in receiving mode [9]*

When the load impedance of load and impedance of antenna are complex conjugate of each other, impedance is matched. All the power is transferred when input impedance and source impedance are perfectly matched [11]. To attain the perfect matching, different type of impedance matching techniques can used. To calculate the mismatch between antenna and load, power transmission coefficient can be used, as expressed in equation (2.31) [12].

$$\tau = \frac{4R_L R_A}{|Z_L + Z_A|}, \tag{2.31}$$

where Z_A and Z_L are impedances of antenna and load respectively, expressed as,

$$Z_A = R_A + jX_A \tag{2.32}$$

$$Z_L = R_L + jX_L \tag{2.33}$$

As, $\tau = 1 - |\Gamma|^2$ therefore the relation between reflection coefficient and impedances of load and source can be expressed as below [13],

$$\Gamma = \frac{Z_A - Z^*_L}{Z_A + Z_L}, \tag{2.34}$$

The reflection coefficient is usually denoted by the symbol gamma. The magnitude of reflection coefficient does not depend on the length of the line. For maximum power transfer impedance matching is key factor. Which implies that inductive impedance of antenna and capacitive impedance of load are complex conjugate of each other to attain the perfect matching. Different type of methods can apply for matching. Introducing the lumped elements, transmission line transformers and modifications in antenna structures are commonly used techniques for matching.

2.4.1 Polarization and Axial Ratio

Polarization is one of the fundamental characteristics of antenna. First, we will understand the polarization of plane waves, then go through the antenna polarization. Polarization of EM waves is the orientation of E field, either fixed direction or varying with time. Polarization of radiated waves vary with the direction as it moves away from the centre of antenna. It means, different parts of radiation pattern may have diversity of polarization. Polarization can be categorized in three types, and the usage of them is depends upon the type of application for which we are using the antenna. An instantaneous field travelling in negative z direction is expressed in equation (2.35) [8],

$$\xi(z;t) = a_x\xi_x(z;t) + a_y\xi_y(z;t) \tag{2.35}$$

Instantaneous components in x and y directions can be expressed as [8];

$$\xi_x(z;t) = Re\left[E_x{}^{-e^{j(wt+kz)}}\right] = E_{xo}\cos(\omega t + kz + \phi_x), \tag{2.36}$$

$$\xi_y(z;t) = Re\left[E_y{}^{-e^{j(wt+kz)}}\right] = E_{yo}\cos\left(\omega t + kz + \phi_y\right), \tag{2.37}$$

$$\xi(z;t) = E_{xo}\cos(\omega t + kz + \phi_x) + E_{yo}\cos\left(\omega t + kz + \phi_y\right), \tag{2.38}$$

where ξ_x and ξ_y are the x and y components respectively. E_{xo} and E_{yo} are maximum magnitudes of x and y axis respectively. Axial ratio (AR) is the ratio of major axis to the minor axis; expressed in equation (2.36) and figure 6 demonstrates major axis, minor axis [9];

$$Axial\ Ratio\ (AR) = \frac{Major\ Axis}{Minor\ Axis} \tag{2.39}$$

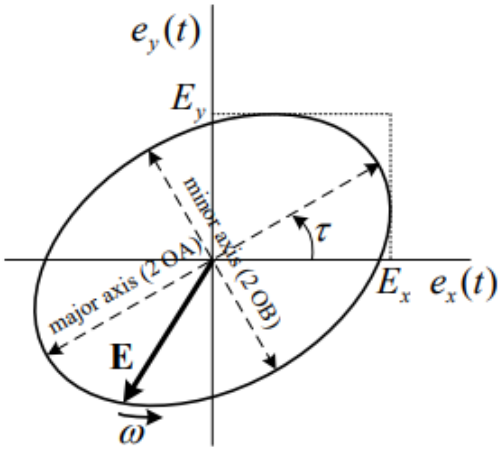

Figure 6. *Polarization ellipse*

Linear Polarization

An electromagnetic (EM) plane wave is characterized by electric and magnetic fields travelling in a single direction when there is no field variation in the two orthogonal directions. In this case electric and magnetic fields are perpendicular to each other and also perpendicular to the direction of plane in which wave is propagating. If the electric field vector always points along a straight line then that EM plane wave is said to be linearly polarized wave. In linear polarization, electric field moves back and forth along a fixed line. Linear polarization can be achieved if the electric field vector possesses only one component or two orthogonal components, in phase with each other or out of phase with multiple of 180°. Figure 7 illustrates the linear polarization.

$$\Delta\phi = \phi_y - \phi_x = n\pi \qquad n = 0,1,2,3 \ldots, \tag{2.40}$$

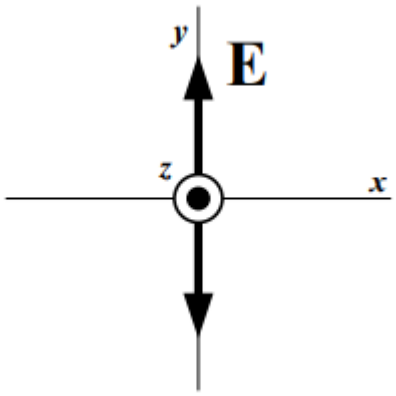

Figure 7. *Linear polarization*

For linear polarization,

$$\mathrm{AR} = \text{infinity } (\infty)$$

Circular Polarization

In circular polarization, E field vector varies in two planes with equal magnitude. Circular polarization can be accomplished if, field vector must have two orthogonal linear components with same magnitude and time-phase difference must be odd multiple of 90°. Such that in equation 2.37.

$$|\xi_x| = |\xi_y|,$$

$$\Delta\phi = \phi_y - \phi_x = +\left(\frac{1}{2} + n\right)\pi \qquad n = 0,1,2,3 \ldots, \tag{2.41}$$

$$\Delta\phi = \phi_y - \phi_x = -\left(\frac{1}{2} + n\right)\pi \qquad n = 0,1,2,3 \ldots, \tag{2.42}$$

where equation 2.41 refers to clockwise and equation 2.42 refers to anti-clockwise rotation.

Circular polarization is illustrated in figure 8 in which the electric field vector remains same but rotates in circular form with a constant angular frequency ω. Right hand circular polarization (RHCP) and left-hand circular polarization (LHCP) are two types of circular polarization depending upon the direction of rotation of angular frequency, clockwise or anti-clockwise respectively. For of circular polarization,

$$\mathrm{AR} = 1$$

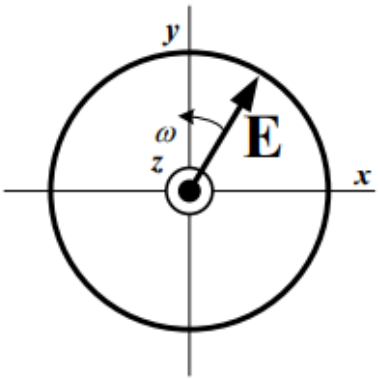

Figure 8. *Circular polarization*

Elliptical Polarization

In case of elliptical polarization, the tip of the electric field vector follows an elliptical trace in space. At any instant, the electrical field vector points the corresponding elliptical locus. The polarization is of two types, right-handed and left-handed if the electric rotates clockwise and counter clockwise respectively. In Elliptical polarization, E field vector varies in two planes but with different magnitudes. Elliptical polarization can be accomplished if, field vector must have two orthogonal linear components with same or different magnitude. If both have same magnitude, the time-phase difference between the orthogonal components must not be odd multiple of 90°, which is the case of circular polarization. If both have different magnitude, the time-phase difference between the orthogonal components must not be zero or multiple of 180°. From the above conditions of accomplishing the elliptical polarization it is concluded that linear and circular polarization are two special cases of elliptical polarization. Elliptical polarization is illustrated in figure 9.

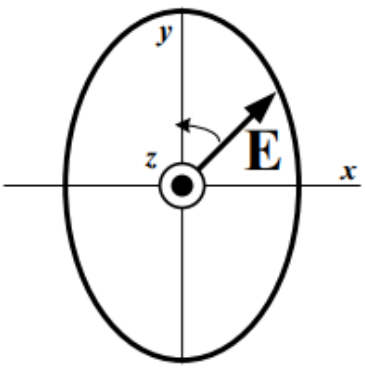

Figure 9. *Elliptical polarization*

For elliptical polarization AR is the ratio of the major to minor component of electric fields, and its value can vary between 1 to ∞ [8].

Polarization Mismatch

The polarization of an antenna is the polarization of the radiated fields produced by an antenna, evaluated in the far field in a specific direction that is typically as that of maximum gain. The polarization of an antenna remains same over the main lobe and differ for minor lobes. Practically, the polarization of the incident wave may differ from the polarization of the receiving antenna. Therefore, the power extracted by the antenna from the incident wave may not be maximum, because of different polarization known as polarization mismatch.

$$\mathrm{E_i} = \widehat{\mathrm{P}}_{\omega}\mathrm{E_i} \tag{2.43}$$

$$\mathrm{E_a} = \widehat{\mathrm{P}}_{\mathrm{a}}\mathrm{E_a} \tag{2.44}$$

where E_i and E_a refer to the electric field of incident wave and electric field of receiving antenna respectively. $\hat{P}_{\omega}$ and $\hat{P}_a$ are unit vectors, also known as polarization vectors. Polarization loss factor (PLF) is the measure of polarization mismatch, which can be defined as,

$$PLF = \left|\hat{P}_{\omega} \cdot \hat{P}_a\right|^2 = |cos\Psi_P|^2, \tag{2.45}$$

where Ψ_{P} the angle between two vectors is forms the angle.

This concept is important for antenna to antenna communication. First, vertically polarized antenna will not communicate with horizontally polarized antenna. Due to reciprocity theorem, antennas transmit and receive in the same manner. Hence, horizontally polarized antenna transmits and receives horizontally polarized fields. Consequentially, when PLF is 0, no power is transferred, whereas, when PLF is 0.5 half of the power is transferred. In case of maximum power transfer, PLF is unity.

2.5 Friis Transmission Equation

One of the fundamental equations to understand the line of sight path loss between two antennas. This equation tells that how much power an antenna receives, radiated by another antenna, in ideal conditions. It can be expressed as [9],

$$\frac{P_r}{P_t} = e_{rr}D_r e_{rt}D_t(1-|\Gamma_r^*|^2)(1-|\Gamma_t^*|^2)(\frac{\lambda}{4\pi \mathrm{R}})^2 PLF, \tag{2.46}$$

where R is the distance between two antennas. And it must satisfy the condition,

$$R > \frac{2D^2}{\lambda}$$

where D is the largest dimension of either antenna. The subscripts t and r represent transmitting and receiving antennas respectively. A simple radio communication link is shown in figure 8.

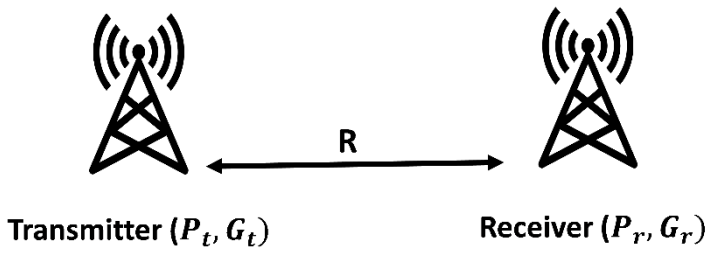

Figure 10. *A simple radio communication link*

The term $(\frac{\lambda}{4\pi R})$ is known as free space loss factor, which measures the spherical spreading losses of antenna. By taking two assumptions into account, no reflection between antennas and same polarization, the Friis equation can be expressed in simple form,

$$\frac{P_r}{P_t} = G_r G_t (\frac{c}{4\pi R})^2 = G_r G_t (\frac{\lambda}{4\pi f R})^2 \quad (2.47)$$

3. BASICS OF RF ENERGY HARVESTING SYSTEMS

3.1 Overview of Radio Frequency Energy Harvesting System

At the beginning of 20th century, Nikola Tesla introduced the concept of wireless power transfer and harvesting the energy [14] and later in 1969 Brown experimented that if high power transmitter is used as power source then a small helicopter can be RF-powered [15]. Energy harvesting is a technique to convert the captured energy from environment to useable electric power. RF energy harvesting is the most attractive harvesting technique because of the abundance of RF signal, especially in urban areas where radio, television broadcast, cellphone services and wireless local area network (WLAN) are redundant and readily available as an ambient energy source [16]. It also provides a long-term solution to low powered wearable electronic devices, RFID systems, human body implantable devices, wireless sensor network (WSN), internet of thing (IoT) devices [16] [17].

According to RF energy harvesting concept, when wireless power radiates in free space, this power can be converted into direct current (DC). Wireless power transfer (WPT) can be divided in inductive coupling, magnetic resonance coupling and RF energy harvesting. An electric transformer is an example of inductive coupling in which alternating current in a primary coil generates a varying magnetic field that another coil can use to harvest power. The magnetic field strength decay with a factor of $\frac{1}{r^3}$ which strictly limit the range, where r is the distance from wire (antenna). Magnetic resonant coupling is an improvement of the inductive coupling with an efficiency up to 40%. Although inductive coupling and magnetic resonance coupling have the high power conversion efficiency, it is appropriate only for near field energy harvesting system applications. Rf energy harvesting have met this limitation and it uses for the far field. RF energy harvesting system consists of an antenna to capture the electromagnetic (EM) waves from environment. A rectification module (based of diodes/transistors) to convert the RF power into DC voltage. The RF spectrum includes the frequency ranges from 3 kHz to 300 GHz [18] [19].

Figure 3.1 demonstrates the fundamental blocks of an RF energy harvesting system. It comprises of an ambient RF source, an impedance matching network, a rectification module and an energy storage. RF rectifier unit harvests the RF signals from environment to convert into DC voltage and to store the energy by charging in the storage capacitor. Power transmitted by RF source, the distance between RF source and receiving antenna, the gain of RF source antenna and receiving antenna, path-loss component and RF-to-DC conversion efficiency are the factors which determine the amount of electrical power to be harvested [20].

Each block of RF energy harvesting system is explained subsequently.

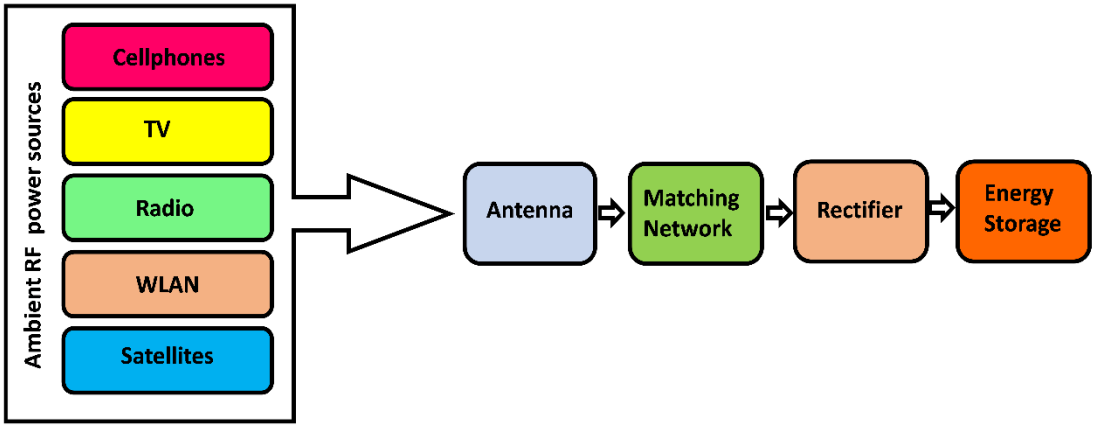

Figure 11. *Block diagram of RF energy harvesting system*

3.2 Radio Frequency Power Sources

An antenna acts as an RF power source which captures the EM waves within the rich environments of RF signals. Pervasive distribution of wirelessly operated communication networks in metropolitan and urban areas provide a comparatively strong and reliable ambient RF source despite of some traffic fluctuation and some unpredictable behaviour of radio wave propagation [21]. RF antenna can capture energy from different sources; TV signals, GSM 900/1800 bands, 3G (2110-2117MHz), WiFi (2400-2500MHz) and local area network ((LAN) 2.45GHz/5.8GHz) [22]. It is critical to note that the ambient RF sources are accessible in bot indoor and outdoor environment with different frequency bands and polarization. However, to do the prototype measurements an alternative source can be used i.e. RF signal generator to provide the smooth and continues RF signal.

3.3 Impedance Matching Networks

Impedance matching plays an important role in maximum power transmission and improve the power conversion efficiency of the whole system. If the input impedance of the RFEHS antenna is not equal to a complex conjugate of the ambient RF source antenna impedance, impedance mismatch will occur. Impedance mismatch leads to reflect back a part of the RF incident power. Thus, the available power transmitted to the rectifier will be decreased, which results in a lower power conversion efficiency (PCE) [9].

The challenging part in designing an RF energy harvesting system is the impedance matching network. Due to the non-linearity of the rectifier elements, input impedance of the harvester varies as a function of the incident power and frequency [23]. The most convenient approach to cope with this problem is utilizing reactive components in different structures of impedance matching networks including an L, Π and T networks [24].

A simple L matching network consists of a capacitor and an inductor, arranged in any of the eight combinations as shown in figure 12. The series reactance L and shunt reactance C configuration of an L matching network is suitable, If the desired load impedance has inductive impedance values that resides within the conductance circle which passes through the origin or capacitive impedance values that reside outside the resistance circle which passes through the origin. In this case, the series reactance L changes the value of impedance along a constant resistance circle until it meets the unit conductance circle. Then the shunt reactance C of this network changes the value of impedance along a unit conductance circle up to the 50-ohm impedance matching point as shown in figure 12 (a) [25].

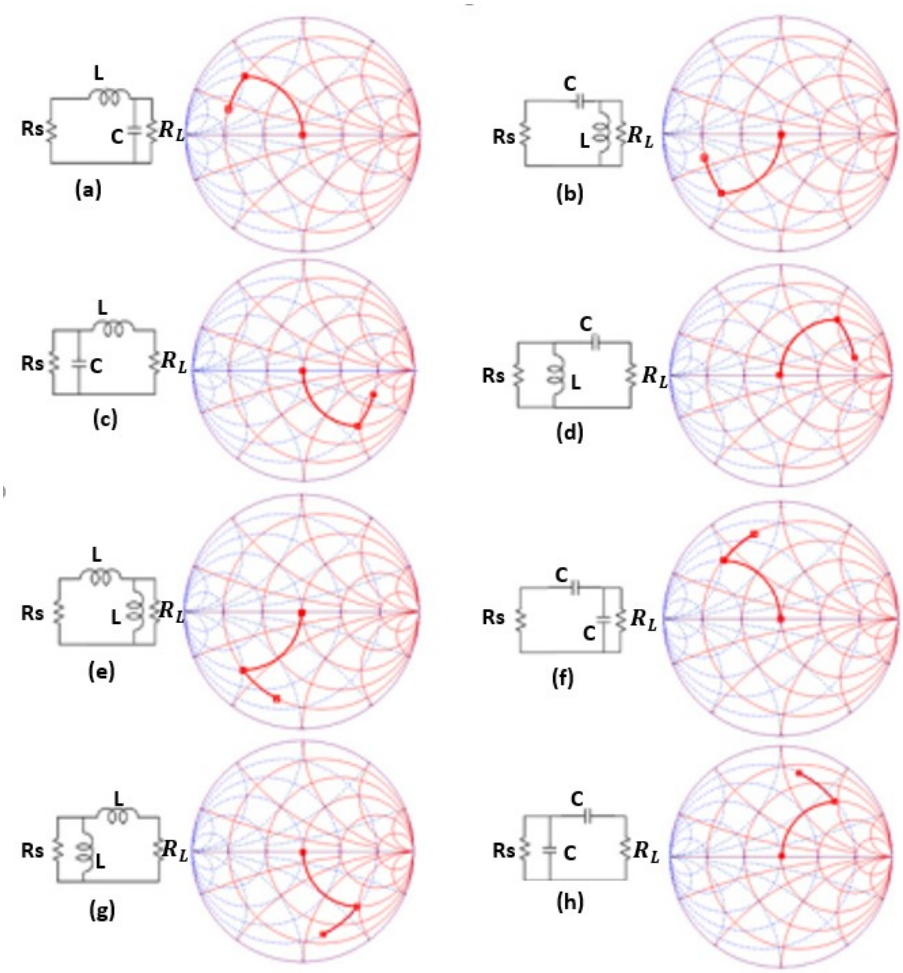

Figure 12. *L-impedance matching network topologies [25]*

Similarly, the series reactance C and shunt reactance L configuration of matching network is utilized where the desired load impedance includes the capacitive impedance values that located inside the conductance circle which passes through the origin or capacitive impedance values that placed outside the resistance circle which passes through the origin. In this case, the series reactance C modifies the impedance value along a constant resistance circle until it reaches to the unit conductance circle. Then the shunt reactance L of this network varies the impedance value along a unit conductance circle up to the 50-ohm impedance matching point as shown in figure 12 (b) [25].

In the arrangement of L matching network, the shunt reactance L makes the impedance value change along a constant conductance circle until it reaches to the resistance unit circle. Then series reactance C of this matching network modifies the value of impedance along the resistance unit circle to the 50-ohm impedance matching as shown in figure 12 (c). This combination can only match the inductive impedance values that situated inside the resistance unit circle which passes through the origin or capacitive impedance values that located outside the resistance unit circle which passes through the origin. In a similar way, in the arrangement of L matching network, the shunt reactance C varies the impedance along a constant conductance unit circle until it intersects the resistance unit circle. Then series reactance L of this matching network makes changes to the impedance value along the resistance unit circle to the 50-ohm impedance matching as shown in figure 12 (d). This element arrangement can only match the capacitive impedance values resided within the resistance unit circle which passes through the origin or inductive impedance values that placed outside the resistance circle which passes through the origin [25].

Every L matching network does not guarantee the required impedance matching. Any matching network can only be used to attain the target impedance circle on the smith chart to a limited extent. Which means there is a bandwidth limitation for any matching network. An L matching network with capacitive reactance is only able to match with inductive impedances located outside the resistance circle and conductance circles passing through the origin. Likewise, an L matching network only with inductive reactance is capable of matching with capacitive impedance situated outside the resistant and conductance circles passing through the origin. The prohibited and alowable areas for several configurations of L matching network from figure 12 are illustrated in figure 13 (a) and(b) respectively. Each of these configurations has some forbidden areas where impedance cannot be achieved [25].

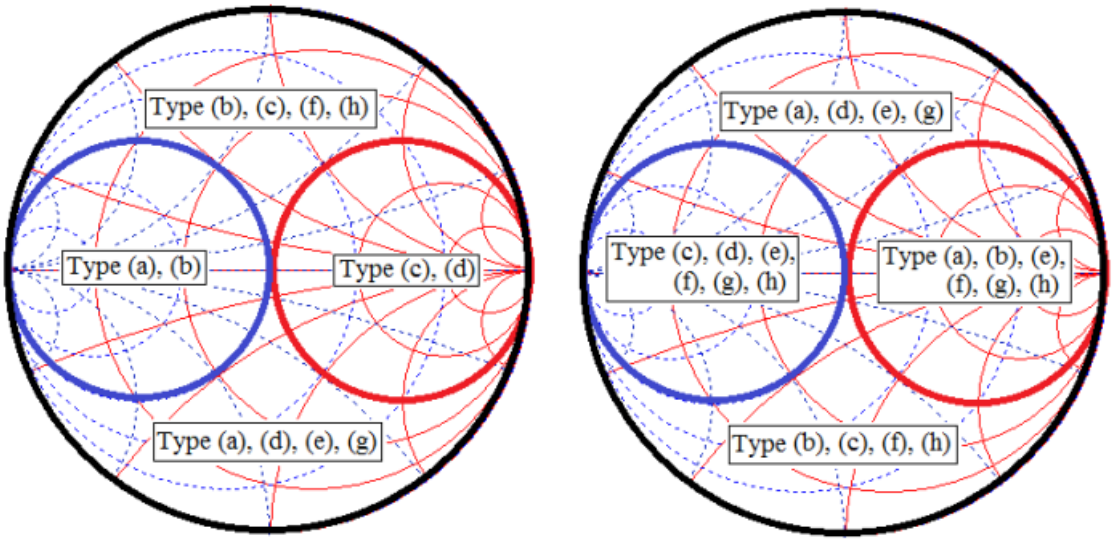

Figure 13. (a) *Permissible* ***(b)*** *Forbidden areas for L-matching networks [25]*

The term matching efficiency ($\eta_{matching}$) is introduced to evaluate the impedance matching between the input impedance of the RF rectifier and the antenna. Matching efficiency is expressed by [26],

$$\eta_{matching} = 1 - |\Gamma|^2 \ , \tag{3.1}$$

where Γ is reflection coefficient and is calculated by [9],

$$\Gamma = \frac{Z_{RFEHS} - Z^*_{antenna}}{Z_{RFEHS} + Z_{antenna}} \tag{3.2}$$

where Z^* indicates the complex conjugate of antenna impedance. It is discussed earlier in chapter 2 [9] that matching efficiency will be maximum when impedance of both systems is complex conjugate of each other, $Z_{RFEHS} = Z^*_{antenna}$.

3.4 Transmission Line Theory

Transmission line theory is more concerned with electrical size. In transmission line theory physical size of network is compared with the wavelength of the signal. On the other hand, in the circuit theory, it is taken as an assumption that dimensions of a network are smaller than wavelengths in size. Transmission line is a distributed parameter network, where current and voltage may vary in phase and magnitude over length. Lumped-element equivalent circuit of short transmission line is shown in figure 10 [1].

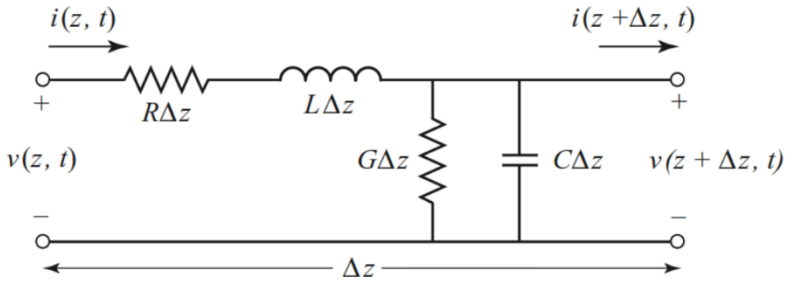

Figure 14. *The equivalent circuit of the lumped element in a short transmission line [1]*

Wave equations of voltage (V) and current (I) are expressed below [1]:

$$V(z) = V_o^+ e^{-\gamma z} + V_o^- e^{\gamma z} \ , \tag{3.3}$$

$$I(z) = I_o^+ e^{-\gamma z} + I_o^- e^{\gamma z}, \tag{3.4}$$

where term $e^{\gamma z}$ represents the wave propagation in Z direction and term $e^{-\gamma z}$ represents the wave propagation in Z direction. And γ is the complex propagation constant, which can be calculated by [1],

$$\gamma = \alpha + \beta = \sqrt{(R + j\omega L)(G + j\omega C)} \tag{3.5}$$

where,

R = series resistance per unit length $\left[\frac{\Omega}{m}\right]$

L = series inductance per unit length $\left[\frac{\mathrm{H}}{m}\right]$

G = shunt conductance per unit length $\left[\frac{\mathrm{S}}{m}\right]$

C = shunt capacitance per unit length $\left[\frac{\mathrm{F}}{m}\right]$

Terminating the transmission line by an arbitrary load impedance, leads to mismatch between transmission line and the impedance of the load. Hence, the waves will be reflected. As a result, the reflection coefficient can be expressed in terms of reflected voltages as [1],

$$\Gamma = \frac{V_o^-}{V_0^+} = \frac{Z_L - Z_0}{Z_L + Z_0} \tag{3.6}$$

where Z_L is the proportional of incoming voltage to its current across the load and the impedance of transmission line (Z_o) can be calculated by,

$$Z_o = \frac{V_o^+}{I_o^+} = \sqrt{\frac{(R + j\omega L)}{(G + j\omega C)}} \tag{3.7}$$

When $Z_L \neq Z_o$, superposition of incident and reflected waves can create standing waves. So, another parameter standing wave ration (SWR) can also be used to measure the mismatch. SWR can be expressed as [1],

$$SWR = \frac{V_{max}}{V_{min}} = \frac{1 + |\Gamma|}{1 - |\Gamma|} \tag{3.8}$$

Return loss is a mismatch between impedance of the antenna and impedance of the source, in this condition some of the transmitted power is reflected. Generally, the threshold of return loss is -10dB, which depicts that 90% of the incident power is transmitted. Return loss can be computed as [9],

$$RL_{(dB)} = -20log_{10}\,|\Gamma| \tag{3.9}$$

3.5 RF Rectifier

RF rectifier is utilized to convert the captured RF signal by an antenna into a stable DC output. It is a fundamental block of the RF energy harvesting system, which recently most of the research is conducted to improve the sensitivity of the rectifier. Choosing the appropriate architecture of the rectifier mostly depends upon the input RF signal, frequency and the desired output voltages. Power conversion efficiency (PCE), circuit size,

leakage current, threshold voltage, sensitivity, rise time and ripples are the required characteristics, which are taken into account for the better performance of the rectifier. All these characteristics are explained one by one [27].

Sensitivity of the rectifier is the minimum amount of input power required to attain a certain value of DC output voltage and to achieve a desired efficiency level. Threshold voltage of rectifying elements has effects on the efficiency of the rectifier. Rectifier with more appropriate sensitivity can be achieved by lower threshold voltage of the rectifying components. High sensitivity leads to rectify the harvested RF signal with low power level. Rise time is the required time to reach the 90% of the final output voltage level which depends on the load and capacitor. Fast time rise is required to guarantee that there is no delay in the system. The rectified output DC voltage have some undesired ripples and noise. Small or no ripples ensure the smooth and stable DC output voltage, which could be achieved by the high value capacitor.

The overall efficiency of the rectifier of RFEHS is the ratio of the output DC power to the input power. It is expressed in (3.10) [29],

$$\eta_{EH} = \frac{P_{outDC}}{P_{inEH}}, \tag{3.10}$$

where output DC power P_{outDC} is obtained after rectification across the load and P_{inEH} is the power captured by the RF energy harvesting unit. P_{outDC} can also be expressed as (3.11) [23].

$$P_{outDC} = \frac{V^2{}_{outDC}}{Z_L}, \tag{3.11}$$

where Z_L is the load across the output power. It can be a resistor, capacitor, inductor, or their combination.

Diode is a key component of a rectifier. In a rectifier circuit, diode is responsible for RF to DC conversion, and mostly the efficiency depends upon the diode(s). Saturation current, junction capacitance and its conduction resistance are the characteristics of a diode which determines the performance of the rectifier [28]. In general, silicon Schottky diodes are used because of their lower threshold voltages and low junction capacitance.

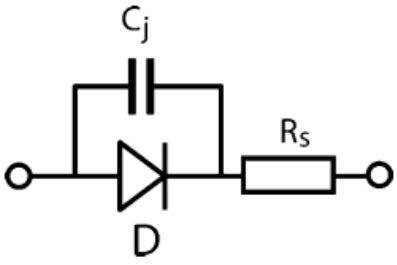

Figure 15. *Electric circuit for the Schottky diode [31]*

The model of Schottky diode consists of a substrate resistance R_s, junction capacitance C_j and a non-linear diode D, which has voltage-current characteristics given by,

$$i_D = I_s(e^{\alpha v_D} - 1), \tag{3.12}$$

where i_D the current passing through diode, v_D is the voltage across diode, I_s is the saturation current and $\alpha = {}^{q}/_{nkT}$ is the reciprocal of thermal voltage. Here, q is the charge of electron, T is the temperature in Kelvin and n is the diode ideality factor [29]. A half-wave rectifier, full-wave rectifier and voltage multiplayer are different approaches a for producing DC voltage [30].

Half-wave and Full-wave Rectification

In half wave rectification, only positive or negative half cycle of the AC input signal passes through the diode. So, we only get half cycle at the output voltage as shown in figure 16. In this method, half of the power is rectified. In full wave rectification both positive and negative half cycles are rectified and available as output voltage as shown in figure 17. Rectification power of full wave rectifier is double than half-wave rectifier [31].

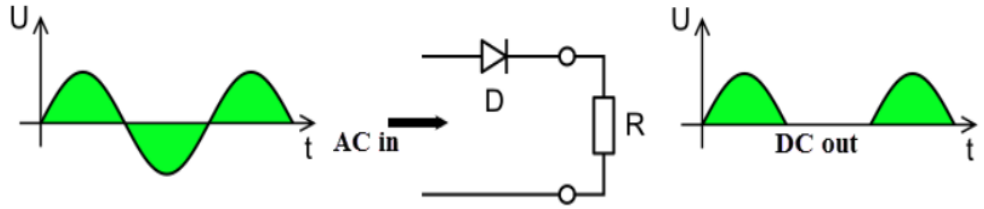

Figure16. *Half-wave rectification*

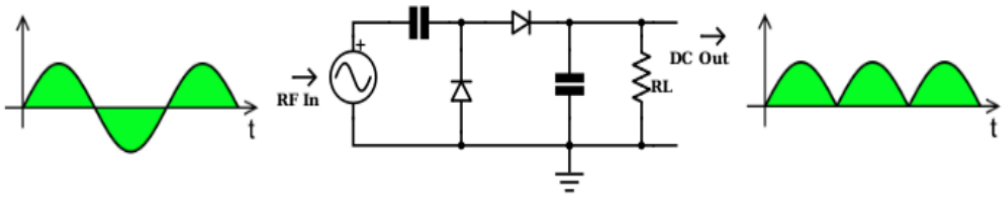

Figure 17. *Full-wave rectification*

Voltage Doubler

One of the most common rectification topologies is a voltage doubler, which not only rectify the voltage but also doubles the input voltage. This circuit consists of two capacitors and two diodes as shown in figure 18. During the negative half cycle of the input signal, diode D_1 is forward biased and capacitor C_1 is charged to the negative input peak value (V_P).

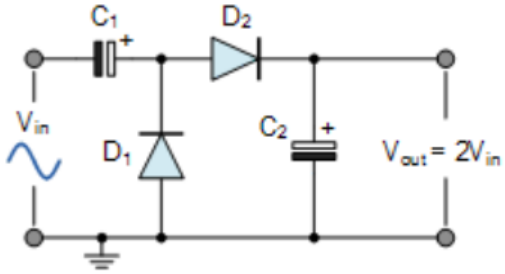

Figure 18. *Simple voltage doubler*

Similarly, during the positive half cycle of the input signal, diode D_2 is forward biased and capacitor C_2 is charged to the positive input peak(V_P). In this condition, diode D_1 is reverse biased which allows to discharge the capacitor C_1 through diode D_2. In ideal condition, at output of capacitor C_2 we get double voltage which is the sum of negative and positive input peak voltages. Threshold voltages of diode (V_{th}) reduce the output voltageand it is subtracted from the peak voltage (V_P), as expressed in the equation 3.13. By adding the N stages of capacitor-diode, the output voltages can also be increased, according to the application. This output voltage of N-stages is expressed in 3.14 [32].

$$V_{out} = 2\ (V_P - V_{th}) \tag{3.13}$$

$$V_{out} = 2N\ (V_P - V_{th}) \tag{3.14}$$

Dickson and Villard Charge Pump

Dickson charge pump and Villard voltage multiplier are two common voltage multiplier topologies based on diodes. Basically, both topologies consist of voltage doubler cells in different number of stages. In Dickson charge pump, the of voltage doubler cells are connected in parallel while in Villard voltage multiplier the voltage doubler cells are connected in series. Dickson charge pump is basically a DC to DC converter with two clocked inputs. By shorting the DC input signal and one of the clocked lines to the ground plane, this DC to DC converter can become an RF rectifier [33]. A charge pump is not only converting RF power to DC voltage but also multiply the voltage according to the number of stages. However, increasing the number of stages results in enhancing the power loss and reducing the total power efficiency. Schematics of Dickson charge pump and Villard voltage multiplier are illustrated in figures 19 and 20, respectively [34].

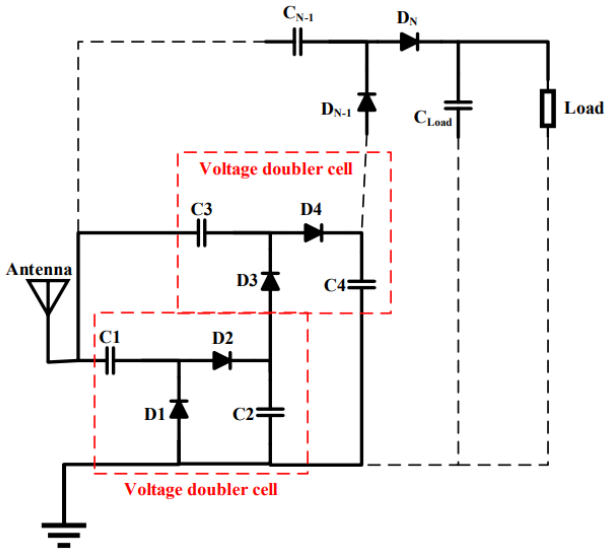

Figure 19. *Schematic of Villard voltage multiplier [34]*

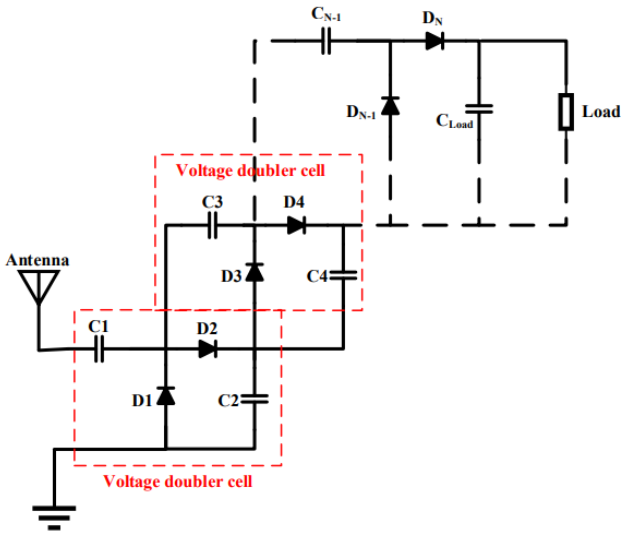

Figure 20. *Schematic of Dickson charge pump [34]*

3.6 Energy Storage

Energy storage unit is the last block of the RF energy harvesting system. Rechargeable batteries and capacitors are used for storing the produced DC voltage. Moreover, the size of capacitor and battery depends upon the desired voltages of application. Different energy storage components and their characteristics are studied to choose the suitable candidate for energy storage, considering their advantages, disadvantages and other features according to the application. Generally, to store the rectified RF power into DC voltage, a capacitor is utilized in Villard and Dickson charge pumps in parallel with the load, as illustrated in figure 19 and 20. This capacitor not only stores the energy but also smoothen the DC output voltage, as explained in section 3.5.

Supercapacitors

Supercapacitor or ultracapacitor are components used for energy storage. These supercapacitors are also known as electrochemical double-layer capacitors (EDLC) due to storing electrical energy in electrolytic double layer. Ceramic and electrolyte capacitors show higher power density but lower energy storage density. The two remarkable characteristics of this new technological component includes higher capacitance value and capability of charging and discharging very fast due to lower internal resistance. Therefore, these features make supercapacitor a strong candidate in field of industrial and power electronics for energy storage purposes. ECLDs may supply hybrid vehicles and may also use in toys' industry and it would be a better economic approach for uninterrupted power supplies (UPS) [35].

A supercapacitor cell essentially comprises of two electrodes, an electrolyte and a separator. Electrochemical materials are used to provide the maximum surface area for maximum production of electrolyte ions. As a result, higher capacitance is achieved as the capacitance depends upon surface area. Electrolyte can be of any solid state, organic or aqueous type according to the application. ECLD is one of the promising charge storage devices having characteristics of low electrodes thickness but high electrode surface, low separator thickness with high ionic separator conductance, high ionic electrolyte conductance, high electrode conductance and high electronic separator resistance. Internal structure of supercapacitor during charged and discharged condition is shown in figure 21 [34] [35].

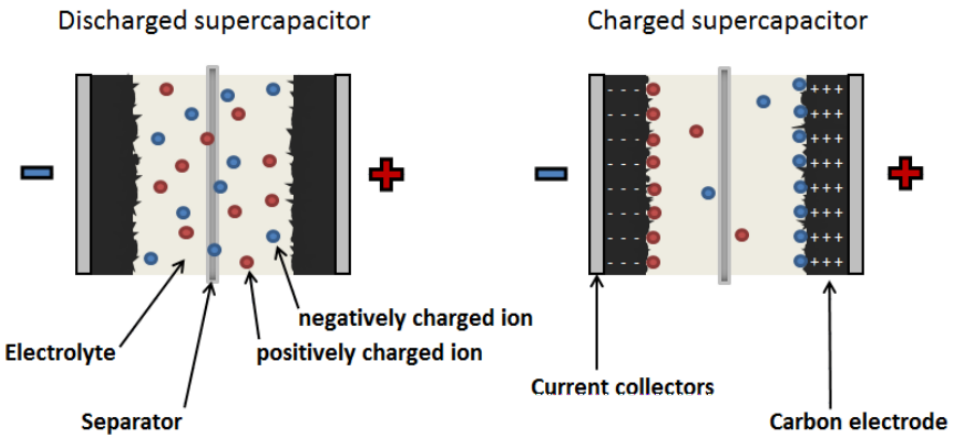

Figure 21. *Internal structure of supercapacitor*

Power electronics and other application devices require energy storage components as small as possible in weight and volume. Supercapacitors fulfill this requirement. Batteries contain high energy storage densities but possesses lower power densities. Although batteries have fast charging-discharching cycle, but it includes limited lifetime. Thus, batteries are not environment friendly and these components need high costs for recycling or neutralizing. Whereas, EDLCs have many advantages over these limitations. Super-

capacitors are environment friendly, durable, reliable, longer in lifetime, and do not require any maintenance. Only disadvantage with EDLCs is their low absorption and high self-discharging. Characteristics of batteries, capacitors and EDLCs are presented in table 1 [35].

Table 1. *Comparison of different characteristics of batteries, capacitors and EDLCs*

	Capacitor	**Batteries**	**EDLCs**
Energy Density [Wh/Kg)	0.1	100	3
Power Density [W/Kg]	10^7	100	3000
Time of charge [s]	$10^{-3} - 10^{-6}$	>1000	0.3-30
Time of discharge [s]	$10^{-3} - 10^{-6}$	1000-10000	0.3-30
Cyclability	10^{10}	1000	10^6
Typical lifetime [years]	30	5	30
Efficiency [%]	>95	70-85	85-98

Lithium Ion Batteries

Lithium ion batteries (LIB) developed in 1912 but became popular in 1991 when Sony adopted this technology. LIBs are usually classified as those batteries in which insertion reaction of lithium ions is utilized, as a charge carrier, for both cathode and anode. Although, different cell chemistries can be utilized according to the energy storage application. So, there is not only a single denotation for lithium ion batteries as in nickel cadmium batteries. LIB batteries consist of two electrodes (positive and negative), separator and electrolyte. Both electrodes form electrochemical cells, which provide lithium ions from anode to cathode and vice versa. Highest energy density with lightest weight is one of the distinguishing factors for these batteries. Efficiency of LIB is approximately 95-98% due to higher electrochemical potential and lower internal resistance. Each electrochemical cell has 3-4 V capacity, which is 1.5 times than nickel metal hydride batteries. LIB have longer lifetime, and high charging and discharging efficiency. Relatively, LIBs have low self-discharging in comparison of nickel cadmium batteries. Li-ion batteries have some disadvantages; manufacturing cost of Li-ion batteries is high; storage capacity of cell reduces over time and performs efficiently only at specific range of temperature [34] [36].

Firstly, Li-ion batteries were used in mobile phone industry, camcorders, laptops and other information technology (IT). Automotive applications are big area of its usage where long life, reliability and safety are required. In automotive industry, Li-ion batteries are not used as starting, igniting and lighting. Their application as traction power sources in hybrid electric vehicles (HEVs), plug-in hybrid electric vehicles (PHEVs), and electric vehicles (EVs) are flourished. Li-ion batteries have significant impact on industrial applications where its application varies from do it yourself (DIY) to specific applications including military, space, and aviation [36].

Lithium Polymer Batteries

Development of lithium ion polymer batteries (LIPB) was started in 1970. Design of LIPB contains dry solid polymer electrolyte and these are desirable source of power for the hybrid electric vehicle (HEV) and electric vehicle (EV) due to its low self-discharging ability and high energy density. Efficiency of batteries is dependent on the size and placement of current collecting tabs and dimensions of electrode. If they are not optimally designed, distribution of potential and current densities will be non-uniform. Lithium ion polymer batteries do not possess good conductivity due to excessive use of electrode metal, which increases its internal resistance. This effect is more prominent if the size of electrode is increased. For higher conductivities, temperature of LIPBs increases that is unnecessary to make it suitable as an energy storage device. Self-discharging is around 1-2 percent per month and no maintenance is required. Due to high energy density and lower power density, LIPBs are very applicable in wirelessly controlling devices and electric vehicles. Some of the major disadvantages of LIPBs are ageing, that is not only dependent on time but also depends on charging-discharging cycle, usually withstand for 1000 cycle. Increasing the energy density of LIBs, causes increase in manufacturing cost. These two factors make it less suitable energy storage device [34] [37].

Solid-State Batteries

Solid-state battery consists of anode, cathode and electrolyte. It works on same technology as lithium-ion battery, but the only difference is, it comprises solid electrolyte instead of liquid electrolyte. High voltages do not allow using liquids solvents as voltage may exceed the decomposition level of water and they create safety issues. Therefore, solid solvents are used to dissolve the supporting salts. Internal resistance of these batteries is reduced due to high ionic conductivity. These kinds of batteries have better safety due to the low vaporization. Some other advantages are wide operation range of temperature, longer lifetime, and ease of miniaturization, high energy density and low power density, which make them suitable candidate for high energy and low power applications i.e. electric vehicles [34] [38].

Consequently, among all the available choices, which are discussed above, supercapacitor is the best choice due to extremely low equivalent series resistance (ESR) and very high charging and discharging rate. Discharge time is in the range of a few seconds. These attributes of supercapacitor are everlasting, which is the objective of our RF energy harvesting system.

4. DESIGN, IMPLEMENTATION AND RESULTS

4.1 Overview of Designed RF Energy Harvesting System

The layout of RF energy harvesting system constrains three major blocks; impedance matching network, rectifier and energy storage unit. Antenna provides the maximum power transfer to the energy harvesting unit. Background study of each block have been discussed in previous chapters. The aim of this work is capturing the RF signal from ambient environment, covert it to DC voltage and energy storage in super capacitor. Figure 22 shows each block of RF energy harvesting system. The system is designed and at 866 MHz, the European UHF RFID spectrum (865.7 MHz to 867.7 MHz). This frequency band convenient for continues wireless power transmission. The designing procedure of antenna and each block RF energy harvesting unit, simulation results and measurement results are presented in following sections.

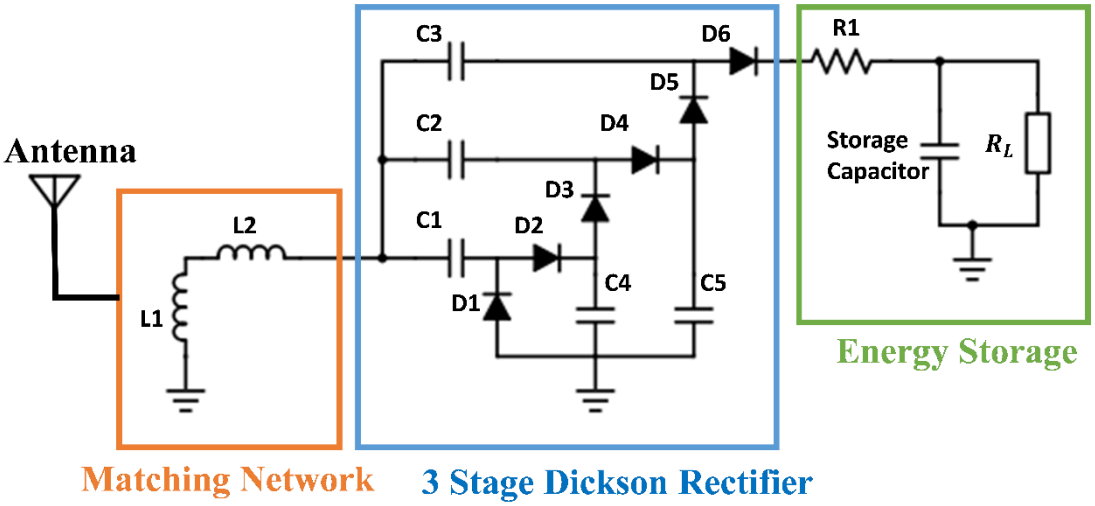

Figure 22. *Block diagram of RF energy harvesting system*

4.2 Designing and Simulations

4.2.1 RF Energy Harvesting Circuit

Antenna, L matching network, Dickson charge pump and energy storage are the blocks of RF energy harvesting system. First, 3 stage Dickson charge-pump is designed for the rectification of the RF input power to the DC output power. We can also increase the number of stages of voltage doubler according to the required DC output voltage. For microwave and RF mixers and detectors surface mount mixers and detector Schottky

diodes are designed with lowest threshold barrier, fast switching speed and zero-bias detectors. Two Schottky diodes SMS-7621-005LS with two capacitors are deployed in each stage of rectifier, as shown in figure 23. Two Schottky diodes SMS-7621-005LS are mounted in one package of SOT-23 series. So, 3 packages of SOT-23 are used in fabrication of rectification unit which reduces the size of circuit [39]. The most imperative part of this RF energy harvesting system is the impedance matching network because a small change in the values of inductors (L) causes significant change in input reflection coefficient and optimized frequency. Energy storage unit comprises a resistor of 56Ω with 11mF capacitor, which is used to determine the time constant. 11mF capacitor is the thinnest and smallest chip type layer capacitor (ELDC), which can charge up to 3.3V. In simulation, the RF signal generator is used at 866 MHz which provides continuous wave as an RF input power source.

SPICE parameters are applied in Advance Design System (ADS) simulator to the diode model by its equivalent circuit. These SPICE parameters are provided by Skyworks and listed in table 5 [39]. In ADS, simplified schematic of Schottky diodes are introduced. Input impedance of rectifier varies as a function RF input power and frequency, due to the non-linear behaviour of Schottky diodes. Harmonic Balance (HB) analysis technique is used in ADS for simulating the DC output voltage of RF energy harvesting circuit versus the RF input power. Large Signal S-Parameter (LSSP) analysis method is a non-linear simulation technique which is used for the study of power dependant behaviour of diodes. Thus, LSSP analysis technique is applied in ADS for the simulation of input reflection coefficient (S11) of RF energy harvesting circuit versus the frequency while sweeping the RF input power levels [40].

Table 2. *SPICE parameters of Schottky diode*

Parameter	Value	Unit
B_V	7.0	V
C_{J0}	0.18	PF
E_G	0.69	eV
I_{BV}	1 E-5	A
I_S	5 E-8	A
N	1.08	-
R_S	6.0	Ω
$B_P(VJ)$	0.65	V
$P_T(XTI)$	2	-
M	0.5	-

The linear circuit model of Schottky diode can be demonstrated as in figure 23 [39].

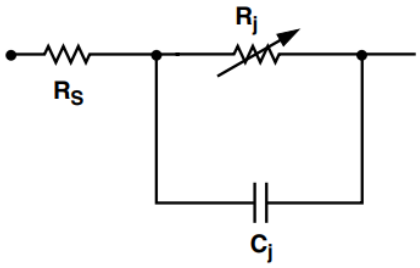

Figure 23. *Equivalent linear circuit model of diode*

where R_S is the series resistance, C_j is junction capacitance and R_j can be calculated by,

$$R_j = \frac{8.33\times10^{-5}nT}{I_b+I_s} \tag{5.1}$$

where I_b is externally applied bias current, I_s is the saturation current, n is ideality factor and T is temperature in Kalvin (K).

Two inductors as an L-matching network are introduced in RF Energy harvesting circuit to minimize the transmission loss and maximize the DC output voltage, as they are associated with matching network. Designing of L-matching network for proper impedance matching between RF power source (antenna) and rectifier plays a crucial role to enhance DC output voltage and to diminish the transmission loss. For this, firstly we fixed the operating frequency at 866 MHz and observe the changes in DC output voltage while sweeping the RF input power level using HB simulation technique. Then, we determine the minimum RF power level at which DC output power level is enough to cross the threshold of a switching diode that is typically 0.85 V. We resolute that RF input power level about 14dBm is required to achieve the threshold of 0.85 V. Figure 24 shows the simulated DC output voltage, with and without matching network.

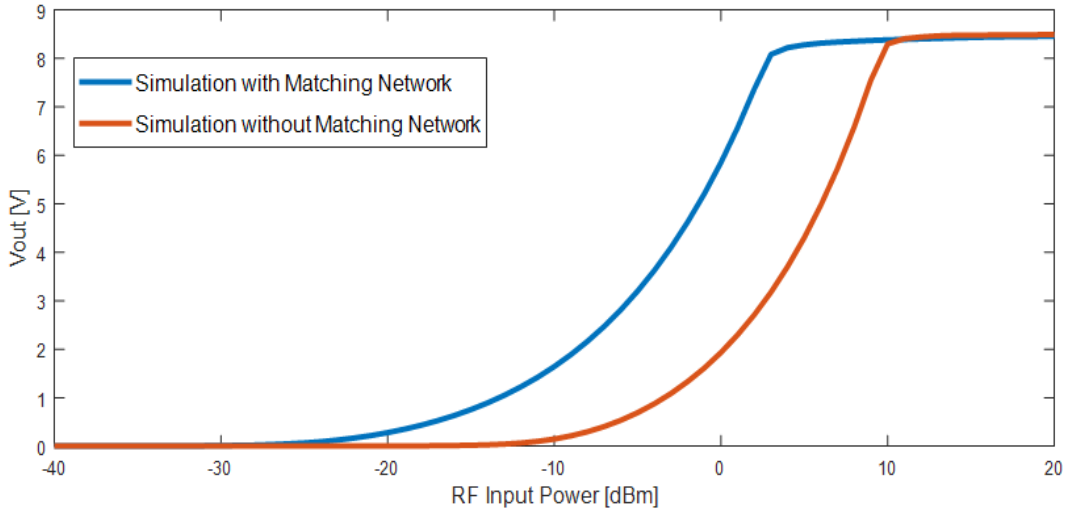

Figure 24. *Simulated DC output voltage of RF rectifier, with and without matching network*

Parasitic behaviour of capacitors and inductors become prominent at higher frequencies. So, the transmission lines are introduced between the RF components. Length and width of transmission line are calculated in ADS by using the FR4 substrate parameter. Then, Input reflection coefficient of circuit while sweeping the frequency at different RF input power levels is simulated by using LSSP analysis technique. Figure 25 demonstrate the simulated input reflection coefficient (S11) of the RF harvesting circuit at 866 MHz frequency with different RF input power levels. Maximum power transmission is achieved at 866 MHz when impedance of RF source and circuit is properly matched. For this purpose, values of inductors used in L-matching network are optimized by varying their values from 1nH to 47n with 0.5 step size. Similarly values of capacitors used in rectification unit and dimensions of transmission lines are also optimized. Length and width of transmission line are 2.96 and 4.75 respectively. Summary of all the components' value used in RF energy harvesting circuit is given in table 3.

Table 3. *Values of components used in RF energy harvesting system*

Component	Value	Unit
$L1$	3.9	nH
$L2$	18	nH
$C1$	82	pF
$C2$	82	pF
$C3$	82	pF
$C4$	82	pF
$C5$	82	pF
$Scottky\ Diode$	SMS-7621-005LS	-
$Storage\ Capacitor$	11	mF
$R1$	56	Ω
R_L (Load)	56k	Ω

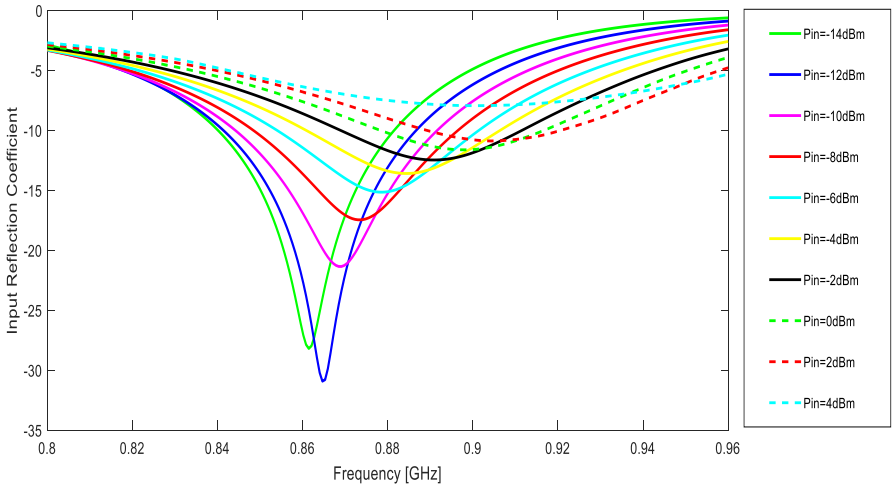

Figure 25. *Simulated input reflection coefficient versus frequency at different input power levels*

4.2.2 Antennas Structure

The antenna structure is simulated ANSYS High Frequency Structure Simulator (HFSS) V.17.1, a full wave electromagnetic field solver based on the infinite antenna elements technique, integral equations for solving a wide range of RF and microwaves.

The main task of designing the antenna is to match the antenna impedance with complex conjugate of RF energy harvesting circuit at desired frequency that is 866 MHz to capture the RF energy from environment. Matching the impedance is very challenging because real part of the impedance is very low so that the real part is very sensitive with the dimensions of feedline. Different materials are considered for this work for simulated in HFSS. Firstly, the antenna is simulated with FR4 epoxy substrate with thickness 1.5784 mm, dielectric constant (ε_r) 4.4 and loss tangent (δ) 0.035. For miniaturization, RT/duroid 5880 is selected as a substrate material which has thickness of 3.175 mm, dielectric constant (ε_r) 2.20 and loss tangent (δ) 0.0004. Geometry of harvesting patch antenna is shown in figure 26.

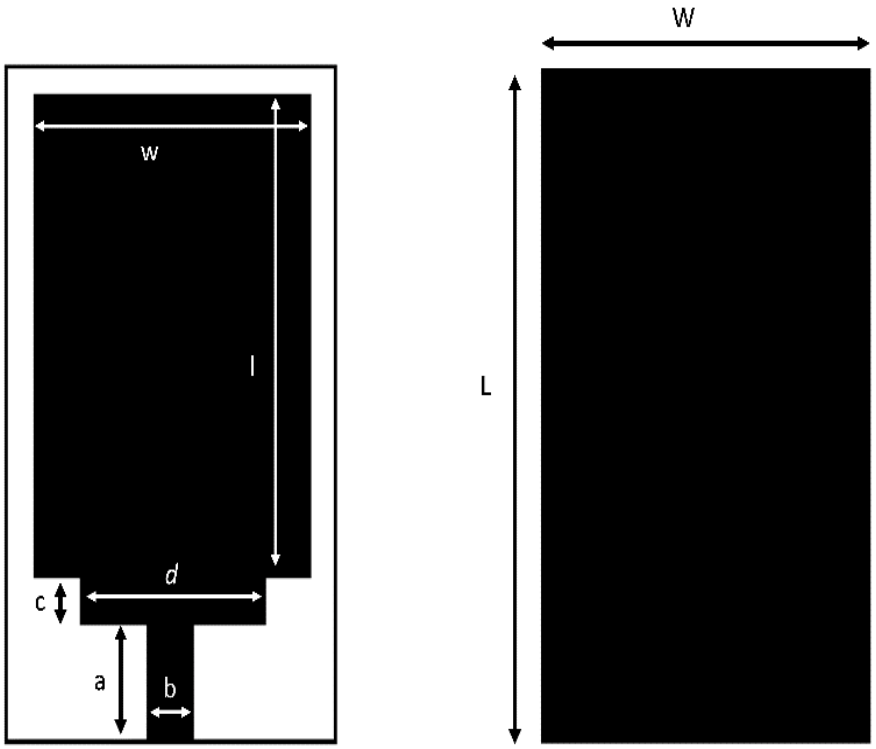

Figure 26. *Geometry of harvesting patch antenna (a) Front (b) Back*

Area of ground plane is optimized to improve the gain of antenna. Antenna is also optimized to match the required impedance and for this purpose changings are done in different geometric parameters like length (a) of feedline, width (b) of feedline, length (c) of strip and width (d) of strip using ANSYS HFSS. List of optimized geometrical parameters is given in table 4.

Table 4. *Geometrical parameters of harvesting patch antenna*

Parameter	Value (mm)
L	178.8
W	100.8
l	121.8
w	60.8
a	25
b	16
c	15
d	32

Figure 27 shows the 3D gain pattern of the harvesting patch antenna at 866 MHz. The RT/duroid 5880 antenna has gain of 5.23 dB with main beam away from the patch antenna that is in the positive z-axis direction. Figure 28 illustrates the power transfer coefficient of harvesting patch antenna. Realistic gain can be calculated by multiplying the simulated gain of antenna by power transfer coefficient of antenna.

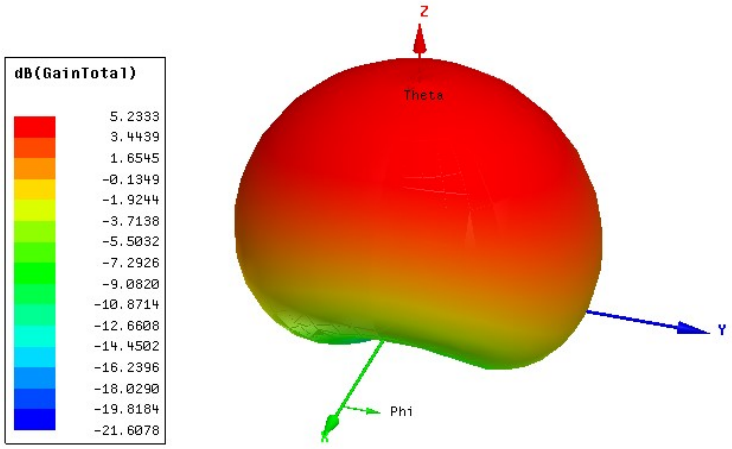

Figure 27. *3D gain pattern of patch antenna at 866 MHz*

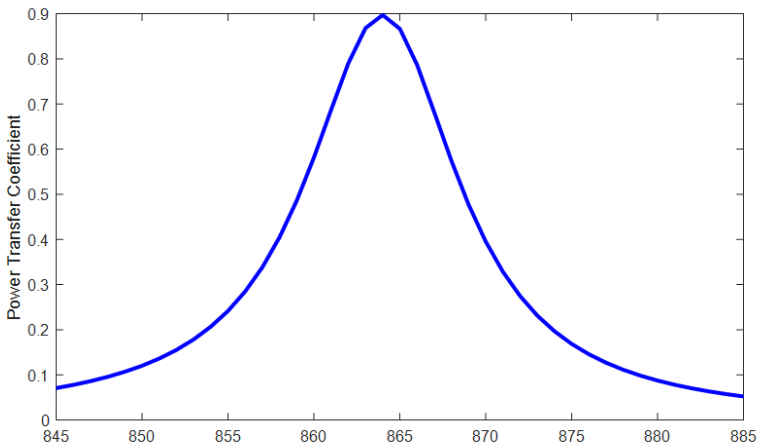

Figure 28. *Power transfer coefficient of antenna*

4.3 Fabrication and Measurement Results

Fabrication of the simulated circuit is done on a FR4 substrate and a 50 Ω SMA connecter is attached with this RF energy harvesting circuit. Vector Network Analyzer (VNA) is used for measurements in which firstly the calibrations are performed within the limit of VNA. To measure the Input reflection coefficient of RR rectifier circuit with matching board, the calibrations are performed for frequency range varies from 0.8 GHz to 0.96 GHz and observes the results through VNA. We also observed the impedance on Smith chart by changing the format from logarithmic to Smith on VNA. Similarly, the input reflection coefficient of RF rectifier circuit without matching circuit is observed via VNA. But, in this case calibrations are performed for frequency range varies from 0 to 4 GHz. We observed from the measurement results that the peak of input reflection coefficient is shifted far away from 866 MHz and peak is also not that negatively large as in simulation results. It is happened because the components of matching network are not properly matched in real circuit and some tuning is required on rectifier circuit board. Figure 29 shows the fabricated RF energy harvester circuit (a) with matching network and (b) without matching network.

After tuning the components of matching network, we observed from the measurement results that by changing the inductor values in matching network. The series inductor in matching network has an impact on the frequency shift of input reflection coefficient and parallel inductor effects the magnitude of input reflection coefficient. To optimize the fabricated RF rectifier circuit to the desired impedance level, the values of series inductor L1 and parallel inductor L2 in matching network are changed by 5.6 nH and 10 nH respectively to obtain the maximum power transfer (MPT) to the RF rectifier circuit at 866 MHz. Impedance of RF rectifier circuit and impedance of antenna are measured by VNA. Figure 30 shows the input reflection coefficient of fabricated RF rectifier circuit with matching network at different input power levels. Figure 31 shows the input reflection coefficient of fabricated RF rectifier circuit without matching network at different input power levels.

(a) (b)

Figure 29. *RF rectifier circuit (a) with matching network (b) without matching network*

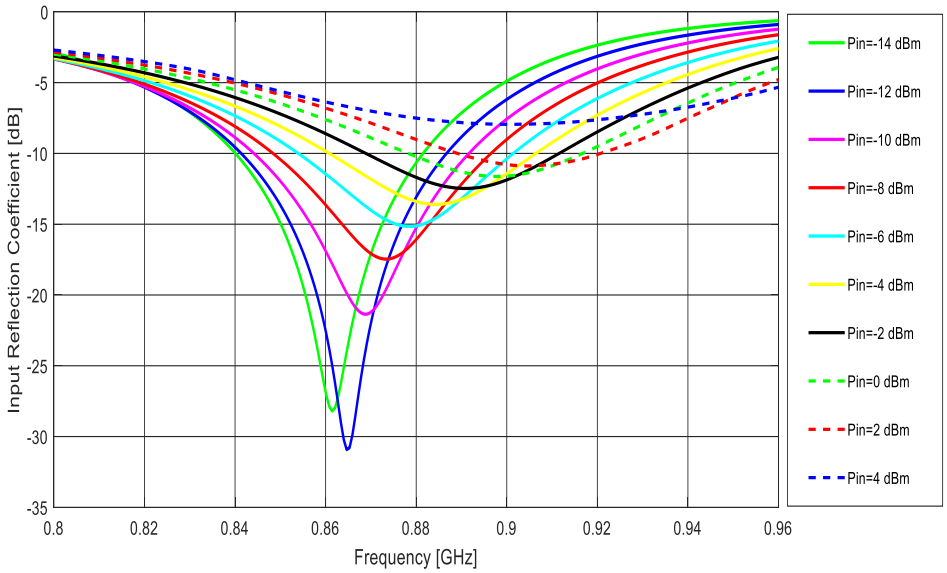

Figure 30. *Input reflection coefficient of RF rectifier circuit with matching network*

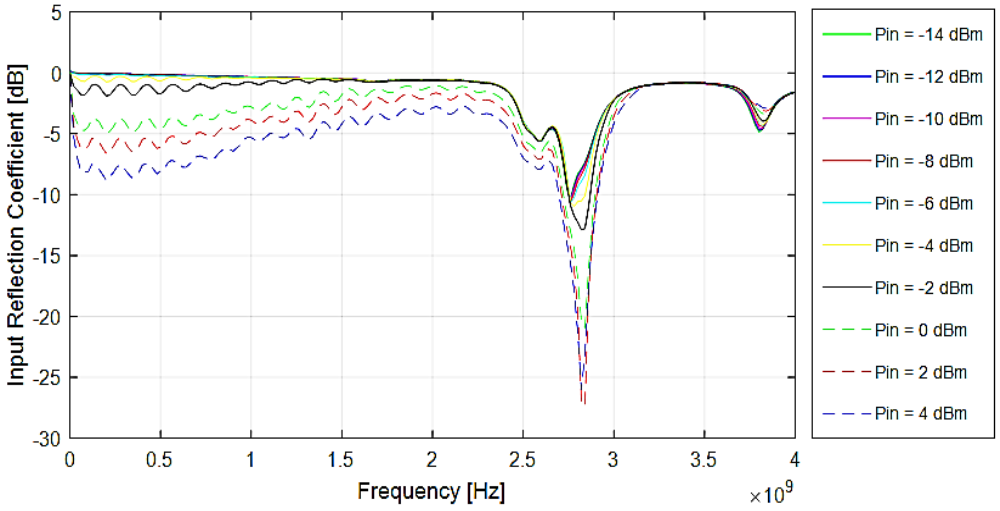

Figure 31. *Input reflection coefficient of RF rectifier circuit without matching network*

Harvesting patch antenna is fabricated on RT/duroid 5880 material. Antenna layout is printed on substrate by placing that into a vacuum chamber and ultraviolet radiations are bombarded. Etching is done by mixture Hydrochloric acid and Nitric acid. In the start, the measured results of the fabricated patch antenna were not accurate as simulated results. As an alternative, instead of fabricating antenna again and again we used copper tape for making layout of patch antenna on RT/duroid 5880 substrate. Because doing modifications by using cutter on copper tape is more convenient. Once the measured results are matched with desired results, the final version of patch antenna is fabricated. We

measured the impedance by using VNA and observed that the results are very close to the desired impedance. Satimo setup is utilized for measurement of antenna radiation as shown in figure 32. In Satimo setup, patch antenna is placed in middle of the rotor which rotates 360 degree during the measurement. There are 15 probes inside the rotor and absorbers surround the antenna to make sure that there will be no reflection of EM waves. Figure 33 shows the comparison between the radiation pattern of harvesting patch antenna and RFID reader antenna.

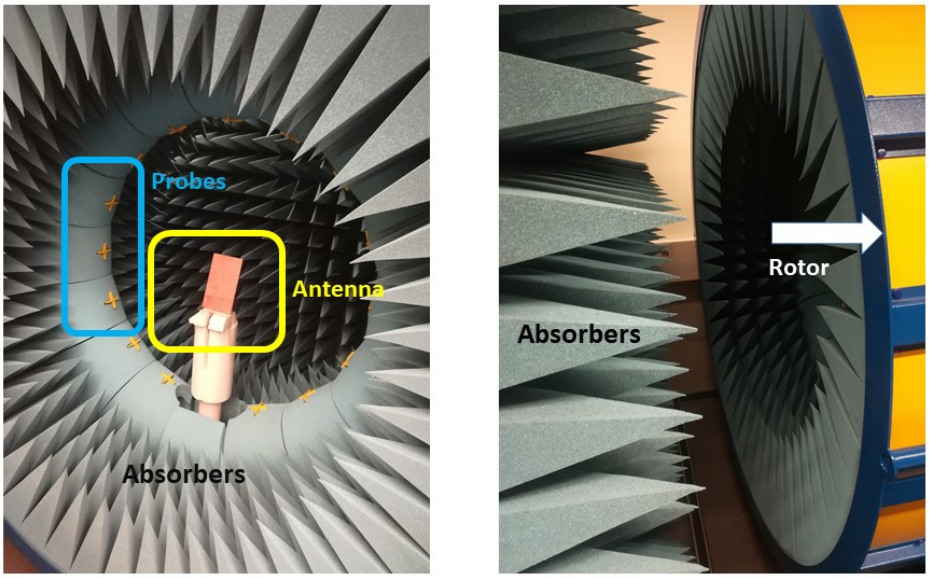

Figure 32. *Satimo setup for antenna measurements*

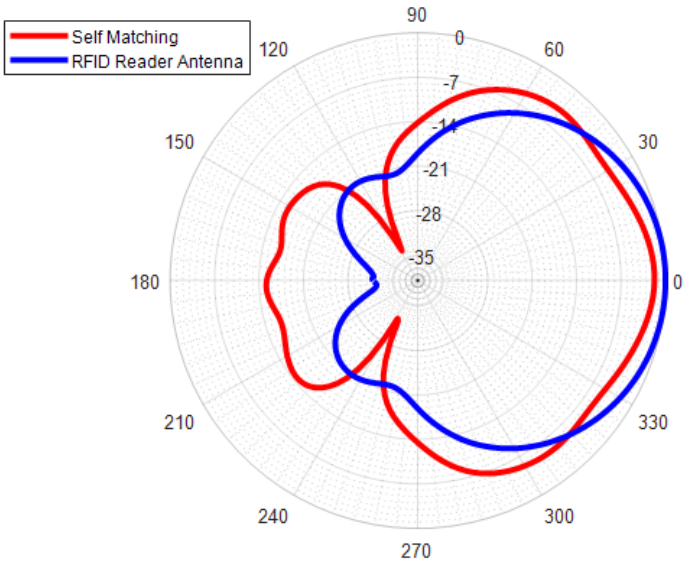

Figure 33. *Comparison of radiation pattern between the harvesting patch antenna and RFID reader antenna*

Performance of the whole system including antenna and RF circuit elavuated by making a setup on Voyantic Tagformance Pro. Figure 34 demonstrate the setup made for the measurement read range and operating bandwith of the RF energy harvesting system and antena. RF energy harvesting circuit is attached with self-matched impedance antenna with the help of SMA connector. Multimeter is attached across the supercapacitor to measure the charging and discharging speed. Voyantic directional coupler which operates at 700-1200 MHz and powered by Voyantic tagformance pro is atteached with reader antenna to transmit the power. When the whole setup is arranged, different power levels are applied to reader antenna to observe the minimum threshold power level at which fabricated antenna capturing the transmissted power by readrer antenna and transferring that captured power to the RF energy harvesting circuit to rectify it. At 28 dBm input power level to reader antenna having gain 12.5 dBi, our system is generating more than 3V at bandwith of 80 MHz varing from 800 to 880 MHz. We observed that charging speed of supercapacitor is higher around centeral frequency, while slower as we measured away from cenetral frequency. Bandwidth of our system is increased when input power level is increased from 28 dBm to 30 dBm. The maximum read range at which our system is charging is 94cm.

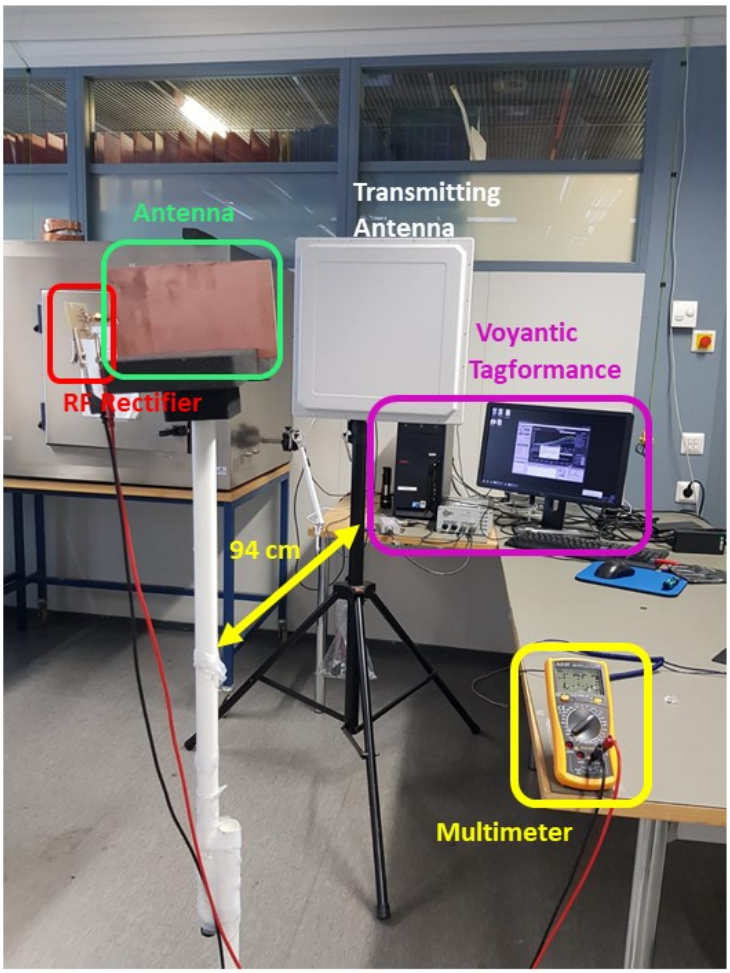

Figure 34. *Voyantic Tagformance pro setup for measurement of the whole RF energy harvesting system including patch antenna*

5. CONCLUSION

The main achievement of this work is that the RF rectifier is directly matched with antenna to avoid the additional matching network. This is the primary approach for these systems to evade the losses because the effect of RF components is prominent at higher frequencies.

In this master's thesis, the design, simulation, and fabrication of RF energy harvesting system are discussed. All the simulations of RF rectifier circuits are done in ADS. Firstly, a three stage Dickson charge pump is simulated by Schottky diodes SMS-7621-005LS. SPICE parameters are applied for modelling diodes in rectifier circuit simulation. RF rectifier converters the RF input power into DC output power. Matching circuit is introduced in RF rectifier circuit, consists of two RF inductors, for proper impedance matching to obtain maximum power transfer (MPT) from source to load. DC output voltage level significantly depends upon the impedance matching circuit and other characteristics, which effects the DC output voltage, are the number of stages in charge pump, storage capacitors, and value of load. The effect of all these parameters are taken into account for designing and simulation. DC output voltage are simulated with and without the matching network. RF signal generator is used in simulation to provide the continuous wave signal, at 866 MHz to the RF rectifier. This system is fabricated on FR4 substrate board.

Other important and crucial part of this thesis work is antenna design which has complex conjugate impedance matching to that RF rectifier impedance, operates at 866 MHz Antenna simulations are done in ANSYS HFSS software and for fabrication RT/duroid 5880 is used as a substrate because it has lower value of dielectric constant and lower value of loss tangent in comparison to FR4.

Measurements are performed on VNA, for both, RF rectifier circuit and harvesting patch antenna to observe the impedance separately. Inductive reactance of patch antenna is conjugate of capacitive reactance of RF rectifier circuit. To observe the overall performance of the whole RF energy harvesting system the setup is made using Voyantic tagformance in which the RF rectifier circuit is connected to patch antenna via SMA connector. Patch antenna is receiving the power from transmitting antenna and transferred to RF rectifier circuit which is converting the received RF power into DC output voltage. The input power level variation has an impact on impedance. Therefore, the RF energy harvesting system should be matched over the range of frequency. Our system has a range of 80 MHz, varies from 800 to 880 MHz, in which the system's output voltage are enough to wake up the RFID IC and other low power level applications.

Despite the fact the whole RF energy harvesting system is verified in both the simulations and the measurements, the improvements can be done RF rectifier circuit design and patch antenna to increase the output voltage level, storage capacity and read range.

6. REFERENCES

[1] D.M. Pozar, “Microwave Engineering”, 4th edition, John Wiley & Sons Inc., The USA, 2011.

[2] W.L. Stutzman, G.A. Thiele “Antenna Theory and Design,” 3rd edition, John Wiley & Sons Inc., The USA: 2012.

[3] I. Zivkovic and A. Murk, “Free-Space Transmission Method for the Characterization of Dielectric and Magnetic Materials at Microwave Frequencies,” Institute of Applied Physics, University of Bern, Switzerland, 14th Nov. 2012.

[4] Peter B.K. Kyabaggu, “Modeling and Characterization of 3D Multilayer Transmission Lines,” The University of Manchester, 2010.

[5] M.N.O. Sadiku, “Elements of Electromagnetics,” 2nd edition, Oxford University Press, 1995.

[6] James C. Rautio and V. Demir, “Microstrip Conductor Loss Models for Electromagnetic Analysis,” IEEE Transaction on Microwave Theory and Techniques, vol. 51 (3), pp. 915 - 921, March 2003.

[7] IEEE, “IEEE Standard for Definitions of Terms for Antennas,” IEEE Transactions on Antennas and Propagation, vol. 17 (7), 2013.

[8] J.D. Kraus, “Antennas for All Applications”, 3rd edition, The USA: McGraw-Hill, 2002. 921 p.

[9] C.A. Balanis, “Antenna Theory: Analysis and Design,” 3rd edition, John Wiley & Sons Inc., The USA, April 2015.

[10] P.V. Nikitin, K.V.S Rao and S. Lazar, “An Overview of Near Field UHF RFID,” 2007 IEEE International Conference on RFID, Grapevine, TX, USA, March 2007.

[11] T. Björninen, “Advances in Antennas, Design Methods and Analysis Tools for Passive UHF RFID Tags,” Tampere University of Technology, Publication vol. 1041, Tampere, 2012.

[12] G. Marrocco, “The Art of UHF RFID Antenna Design: Impedance-Matching and Size-Reduction Techniques,” IEEE Antennas and Propagation Magazine, vol. 50 (1), pp. 66 - 79, Feb. 2008.

[13] K. Kurokawa, “Power Waves and the Scattering Matrix,” IEEE Transactions on Microwave Theory and Techniques, vol. 13 (2), pp. 194 - 202, March 1965.

[14] N. Tesla, “The Transmission of Electrical Energy Without Wires,” Electrical World and Engineer, 1904.

[15] W. Brown, “Experiments Involving a Microwave Beam to Power and Position a Helicopter,” IEEE Transactions on Aerospace and Electronic Systems, vol. AES-5 (5), pp. 692 - 702, Sept. 1969.

[16] Nikta Pournoori, M. Waqas A. Khan, L. Ukkonen and T. Björninen “RF Energy Harvesting System Integrating a Passive UHF RFID Tag as a Charge Storage Indicator,” IEEE International Symposium on Antennas and Propagation, Boston, Massachusetts, USA, July 2018

[17] Kenneth Gudan, S. Shao, J.J. Hull, J. Ensworth, M.S. Reynolds “Ultra-Low Power 2.4GHz RF Energy Harvesting and Storage System with −25dBm Sensitivity,” 2015 IEEE International Conference on RFID (RFID), San Diego, CA, USA, April 2015.

[18] S. Kim et al., “Ambient RF Energy-Harvesting Technologies for Self-Sustainable Standalone Wireless Sensor Platforms,” Proceedings of the IEEE, vol. 102 (11), pp. 1649 - 1666, Nov. 2014.

[19] L. W. Fatih Ünlü, “Energy Harvesting Technologies for IoT Edge Devices,” Helbling Technik AG and Adriana Díaz of ECODESIGN company, July 2018. Available: https://www.iea-4e.org/document/417/energy-harvesting-technologies-for-iot-edge-devices.

[20] D. M. et. al., “Smart RF Energy Harvesting Communications: Challenges and Opportunities,” IEEE Communications Society, vol. 53 (4), pp. 70 - 78, 08 April 2015.

[21] Sika Shrestha, S-K Noh, D-Y Choi “Comparative Study of Antenna Design for RF Energy Harvesting,” International Journal of Antennas and Propagation, Feb 2013.

[22] M. Pareja Aparicio et al., “Radio Frequency Energy Harvesting - Sources and Techniques,” InRenewable Energy-Utilisation and Systems Integration, May 2016. InTech.

[23] C.R. Valenta, G.D. Durgin “Harvesting Wireless Power: Survey of Energy-Harvester Conversion Efficiency in Far-Field, Wireless Power Transfer Systems,” IEEE Microwave Magazine, vol. 15 (4), pp. 108-120, June 2014.

[24] V. Kuhn, C. Lahuec, F. Seguin ja C. Person, “A Multi-Band Stacked RF Energy Harvester With RF-to-DC Efficiency Up to 84%,” IEEE Transactions on Microwave Theory and Techniques, vol. 63 (5), pp. 1768 - 1778, May 2015.

[25] Dr. A. Govind, “Antenna Impedance Matching – Simplified,” Abracon, LLC. Available: https://abracon.com/uploads/resources/Abracon-White-Paper-Antenna-Impedance-Matching.pdf

[26] S. Keyrouz, “Practical rectennas: Far-field RF Power Harvesting and Transport,” Technische Universiteit Eindhoven, Jan. 2014.

[27] Y.C. Wong, P.C. Tan, M.T. Ibrahim, F. Radzi, N.A. Hamid “Dickson charge pump rectifier using ultra-low power (ULP) Diode for BAN applications,” Journal of Telecommunication, Electronic and Computer Engineering, vol. 8 (9), pp. 77-82, 2016.

[28] M.T. Penella and M. Gasulla-Forner, “Powering Autonomous Sensor,” New York, USA: Springer-Verlag, pp. 125–147, 2011.

[29] J.A.G. Akkermans, M.C. van Beurden, G.J.N.Doodeman and H.J. Visser “Analytical Models for Low-Power Rectenna Design,” IEEE Antennas and Wireless Propagation Letters, vol. 4, pp. 187-190, June 2005.

[30] X. Lu, P. Wang, D. Niyato, D. I. Kim and Z. Han, “Wireless Networks with RF Energy Harvesting: A Contemporary Survey,” IEEE Communications Surveys & Tutorials, vol. 17 (2), pp. 757 - 789, Nov. 2014.

[31] S.Y. Mansour, “Design of Multi-Band RF Energy Harvesting System,” March 2018. Available: https://library.iugaza.edu.ps/thesis/123625.pdf.

[32] Electronics Tutorials: Voltage Multiplier. Available: https://www.electronics-tutorials.ws/blog/voltage-multiplier-circuit.html.

[33] D. Schemmel, “A Wireless Energy Harvesting System with Beamforming Capabilities,” Colorado School of Mines. Available: https://mountainscholar.org/bitstream/handle/11124/171006/Schemmel_mines_0052N_11262.pdf?sequence=1.

[34] N. Pournoori, “Wireless Monitoring of a Charge Storage in an RF Energy Harvesting Device,” Master thesis, Tampere University of Technology, Tampere, January 2018.

[35] A. Schneuwly and R. Gallay, “Properties and Applications of Supercapacitors from the State-of-the-Art to Future Trends,” Montena components SA, Rossens, Switzerland, 2000.

[36] T. Horiba, “Lithium-Ion Battery Systems,” Proceedings of the IEEE, vol. 102 (6), pp. 939 - 950, June 2014.

[37] U.S Kim, C.B. Shin and C-S. Kim “Modelling for the Scale-up of a Lithium-Ion Polymer Battery,” Journal of Power Sources, vol. 189 (1), pp. 841-846, April 2009.

[38] K. Takada, “Progress and Prospective of Solid-State Lithium Batteries,” Acta Materialia, vol. 61 (3), pp. 759-770, Feb. 2013.

[39] Sky Works, Data sheet: Surface Mount Mixer and Detector Schottky Diodes. June 2018. Available: https://eu.mouser.com/datasheet/2/472/Surface_Mount_Schottky_Diodes_200041AD-708941.pdf

[40] Agilent Technologies, Diode Detector Simulation using Aligentry Technologies EEs of ADS Software, 1999. Available: https://courses.e-ce.uth.gr/CE433/tutorials/cktsimenv.pdf